GEAP-4480
Informal Research
and Development Report

January 1964

Facsimile Price $ 7.60
Microfilm Price $ 2.51

Available from the
Office of Technical Services
Department of Commerce
Washington 25, D. C.

SODIUM-COOLED REACTORS PROGRAM

# FAST CERAMIC REACTOR DEVELOPMENT PROGRAM

Ninth Quarterly Report

October - December 1963

Prepared for the
United States Atomic Energy Commission
Under
Contract No. AT(04-3)-189, Project Agreement No. 10

Printed in the U. S. A. Price [redacted]. Available from the Office of Technical Information, Department of Commerce, Washington 25, D. C.

ATOMIC POWER EQUIPMENT DEPARTMENT
GENERAL ELECTRIC
SAN JOSE, CALIFORNIA

1660 - TIO-2
1/64

# TABLE OF CONTENTS

## LIST OF ILLUSTRATIONS

# SECTION I

## INTRODUCTION

The Fast Ceramic Reactor Development Program is an integrated analytical and experimental program directed toward the development of fast reactors employing ceramic fuels, with particular attention to mixed plutonium-uranium oxide. Its major objectives are:

a. Development of a reliable, high performance fast reactor having nuclear characteristics which provide stable and safe operation, and

b. Demonstration of low fuel cycle cost capability for such a reactor, primarily through achieving high burnup of ceramic fuels operating at high specific power.

Progress during the period October 1 - December 31, 1963 on the currently active tasks of this program is described in subsequent sections.

This is the ninth in a series of quarterly progress reports written in partial fulfillment of Contract AT(04-3)-189, Project Agreement No. 10, between the United States Atomic Energy Commission and the General Electric Company. Prior progress reports to the Commission under this contract include the following:

Monthly Progress Letters, Nos. 1-47, from July 1959 through November 1963.

GEAP-3888 FCR Development Program - First Quarterly Report, October-December 1961.

GEAP-3957 FCR Development Program - Second Quarterly Report, January-March 1962.

GEAP-3981 FCR Development Program - Third Quarterly Report, April-June 1962.

GEAP-4080 FCR Development Program - Fourth Quarterly Report, July-September 1962.

GEAP-4158 FCR Development Program - Fifth Quarterly Report, October-December 1962.

GEAP-4214 FCR Development Program - Sixth Quarterly Report, January-March 1963.

GEAP-4300 FCR Development Program - Seventh Quarterly Report, April-June 1963.

GEAP-4382 FCR Development Program - Eighth Quarterly Report, July-September 1963.

Supplementary Progress Letters, Nos. 1-9 from October 1962 through November 1963.

Reports from G. D. Collins and W. J. Ozeroff on assignment to CEA-France.

In addition, the following topical reports have been issued:

GEAP-3287 Fast Oxide Breeder - Reactor Physics, Part I - Parametric Study of 300 MWe Reactor Core, P. Greebler, P. Aline, J. Sueoka; November 10, 1959.

GEAP-3347 Fast Oxide Breeder - Stress Considerations in Fuel Rod Design. K. M. Horst; March 28, 1960.

GEAP-3486 Fast Oxide Breeder Project - Fuel Fabrication.
Part I - Plutonium-Uranium Dioxide Preparation and Pelletized Fuel Fabrication, J. M. Cleveland, W. C. Cavanaugh;
Part II - Fabrication of Plutonium-Uranium Dioxide Specimens by Swaging. M. E. Snyder, W. C. Cowden; August 15, 1960.

GEAP-3487 Fast Oxide Breeder - Preliminary Sintering Studies of Plutonium-Uranium Dioxide Pellets. J. M. Cleveland, W. C. Cavanaugh; August 15, 1960.

GEAP-3646 Calculation of Doppler Coefficient and Other Safety Parameters for a Large Fast Oxide Reactor. P. Greebler, B. A. Hutchins, J. R. Sueoka; March 9, 1961.

GEAP-3721 Core Design Study for a 500 MWe Fast Oxide Reactor. K. M. Horst, B. A. Hutchins, F. J. Leitz, B. Wolfe; December 28, 1961.

GEAP-3824 Fabrication Cost Estimate for $UO_2$ and Mixed $PuO_2$ Fuel. G. D. Collins; January 24, 1962.

GEAP-3833 The Post-Irradiation Examination of a $PuO_2$-$UO_2$ Fast Reactor Fuel, J. M. Gerhart; November 1961.

GEAP-3856 Experimental Fast Oxide Reactor, K. P. Cohen, M. J. McNelly, B. Wolfe; November 27, 1961.

GEAP-3876 Plutonium Fuel Processing and Fabrication for Fast Ceramic Reactors, H. W. Alter, G. D. Collins, E. L. Zebroski; February 1, 1962.

GEAP-3880 Comparative Study of PuC-UC and $PuO_2$-$UO_2$ as Fast Reactor Fuel, Part I - Technical Considerations, K. M. Horst, B. A. Hutchins; February 15, 1962. Part II - Economic Considerations, G. D. Collins; November 15, 1962.

GEAP-3885 Experimental Fast Ceramic Reactor Design. Status Report as of October 31, 1961. Edited by K. M. Horst; April 24, 1962.

GEAP-3923 Resonance Integral Calculations for Evaluation of Doppler Coefficients - The RAPTURE Code, J. H. Ferziger, P. Greebler, M. D. Kelley, J. Walton; June 12, 1962.

GEAP-4028 A Fuel Reprocessing Plant for Fast Ceramic Reactors, H. W. Alter; February 1, 1962.

GEAP-4058 Analytical Studies of Transient Effects in Fast Reactor Fuels, R. B. Osborn and D. B. Sherer; August, 1962.

GEAP-4090 FORE - A Computational Program for the Analysis of Fast Reactor Excursions, P. Greebler, D. B. Sherer; October, 1962.

GEAP-4092 Doppler Calculations for Large Fast Ceramic Reactors, Effects of Improved Methods and Recent Cross-Section Information, P. Greebler, E. Goldman; December, 1962.

GEAP-4130 Experimental Studies of Transient Effects in Fast Reactor Fuels, Series I, $UO_2$ Irradiations, J. H. Field; November 15, 1962.

GEAP-4226 Conceptual Mechanical Design of a 565 MW(e) Fast Ceramic Reactor, A. G. Silvester; April, 1963.

GEAP-4271 Measurement of Oxygen-to-Metal Ratio in Solid Solutions of $UO_2$ and $PuO_2$, W. L. Lyon; May 31, 1963.

GEAP-4283 Experimental Studies of Sodium Logging in FCR Fuels G. L. O'Neill; September, 1963.

GEAP-4410 Calculations of Doppler and Sodium Reactivity Effects, P. Greebler; November, 1963.

GEAP-4414 Reactor Safety and Fuel Cycle Economics, K. P. Cohen; November, 1963.

GEAP-4420 Influence of Doppler Effect on Meltdown Accident, N. F. Friedman; December, 1963.

# SECTION II

## SUMMARY

### 2.1 Task B - Vented Fuel Development

Irradiation and post-irradiation examination of the first fission product release experiment capsule B4A, containing a vented-to-coolant fuel pin, was completed. Preliminary examination and analysis of the data show a very promising lack of significant activity in the sodium around the fuel pin even when over half the stable and long lived fission gases were vented from the fuel through the sodium.

A gap conductivity experiment (capsule B5A) has been initiated to determine conductivity of three different possible gap sizes which may be used in an FCR fuel.

### 2.2 Task C - Fuel Testing in TREAT

Transient irradiation of the third 0.25 inch diameter mixed oxide fuel specimen has a target peak fuel temperature, 7000 F, at which dynamic conditions due to clad rupture might be significant to the hazards analysis. Within the accident assumed (110 percent of requested power) a detailed dynamic analysis was completed indicating the transient can be performed with an adequate margin of safety.

Heat transfer and physics calculations have been performed for preliminary design of the first capsule of a series (Series 4) to investigate the mode and effect of possible fuel clad rupture or penetration with high transient energy inputs.

Exposure of the three specimens of the pre-irradiated mixed oxide fuel series have approached 37,000 MWD/T of the planned 50,000 MWD/T target.

### 2.3 Task E - Fuel Performance Evaluation

Fabrication of the larger diameter fuel of reference FCR conditions, capsule E2A, was completed and irradiation started in GETR cycle 50 (December). Thermocouples for use in the initial central fuel temperature measurement capsule, E1A, were received, tested and found to be unsatisfactory, further delaying completion of capsule fabrication.

Preliminary results of the first out-of-pile plutonium migration experiment indicate significant and comparable diffusion of plutonium and uranium in mixed oxide.

## 2.4 Task F - Fast Flux Irradiation of Fuel

Fuel specimen fabrication for the first two assemblies, Groups 1 and 2, scheduled for irradiation in EBR-II is ~65 percent complete. The capsule fabrication and assembly schedule has become very tight since tubing scheduled for delivery from ANL in mid-December contained flaws and had to be rejected when received by ANL from the vendor. A re-order has been placed. Meanwhile, suitable General Electric tubing, purchased for an earlier design, has been shipped to ANL for their examination and check for its possible use.

Planning of the Group 3 fuel preparation is underway preparatory to discussion with ANL.

## 2.5 Task G - Reactor Physics and Core Analysis

Effect of the Doppler coefficient in the core disassembly process following a meltdown accident has been examined and found to reduce the energy release by factors of 10 or more.

Additional computations have confirmed that the Pu-239 Doppler effect is virtually unchanged due to overlapping of U-238 and Pu-239 resonances.

Specifications for a multi-group two-dimensional diffusion theory synthesis computer code have been started.

# SECTION III

## TASK B - VENTED FUEL DEVELOPMENT

### 3.1 Sodium-Fuel Compatability

One Hastelloy-X test capsule was operated with sodium and a $UO_2$ pellet at temperatures of 1000 C for 1 week. The capsule ruptured during operation and the sodium was lost from the container. X-ray diffraction studies on the remaining pellet indicated that most of the original $UO_2$ pellet had oxidized to $U_3O_8$.

### 3.2 Fission Product Plugging

Fabrication of capsule B3A is continuing. The tapered thermal barriers have been received and assembly is underway. The target insertion date for this capsule is GETR cycle 52 (February).

### 3.3 Fission Product Release

#### 3.3.1 Capsule B4A: Vented-Through-Blanket Fuel Pin

The first of three Fission Product Release experiments, capsule B4A, was irradiated for two cycles in GETR at 20 to 24 KW/ft linear power to an accumulative fuel burnup of 14,500 MWD/T. Clad surface temperatures averaged 470 C. The capsule was moved to the RML for immediate examination and disassembly. The subsequent examination and analysis of data collected to date show a most promising lack of significant activity in the sodium around the fuel pin even though a large fraction (over half) of the stable and long-lived fission gases were vented from the fuel and through the sodium.

Although a thorough appraisal of the data is still underway, certain preliminary conclusions can be drawn:

1. A large fraction of the fission gases were released and vented from the fuel. Based on Xe-133 concentrations in small aliquots, a release of about 65 percent was measured and will be assumed until mass spectrograph analysis of stable isotopes from larger gas samples has been completed.

2. The ratio of Xe-133m to Xe-133 in the released fission gas mixture is consistent with a holdup time of the order of days between the point of fission and release from the vent to the gas sample plenum.

3. The predominant activity in the sodium after the decay of Na-24 was Cs-134, an activation product of Cs-133 which is present as a fission product and an impurity.

4. Neither Xe-135 nor Cs-136, resulting from neutron capture by Cs-135, are present outside the fuel pin in significant quantities. Again this is consistent with a long holdup time of the fission gases within the fuel pin and vent. The 6.7-hour I-135 and 9-hour Xe-135 daughter evidently have both decayed below detection levels before the gases were vented.

5. Separations of cesium, rubidium, barium, strontium, and iodine indicate low activity levels in the sodium, but these will require further evaluation and comparison to the sodium control sample now under irradiation as a part of the next capsule in this series (B4C).

6. The majority of the iodine evidently has remained inside the fuel pin and vent system.

### 3.3.1.1 Capsule Description

Capsule B4A contained a vented fuel specimen designed to retain selectively volatile fission products and daughters of short-lived fission gases while releasing stable and long-lived fission gases through 1-13/16 inches of natural $UO_2$ blanket and a diving bell vent situated above the blanket.

The specimen was doubly contained and instrumented with thermocouples in the sodium annulus around the fuel specimen, as well as in the NaK annulus around the sodium container. The capsule is shown in isometric view in Figure 3-1 and schematically in Figure 3-2. The schematic drawing is included to clarify the ensuing discussion of the capsule disassembly.

### 3.3.1.2 Irradiation

The capsule was irradiated in the GETR pool within a vertically adjustable facility tube (VAFT). Thermocouples on the outside of the capsule provided monitoring of the cooling water temperature rise for calorimetric power determinations to guide repositioning of the capsule to follow the axial flux peak. A record of the capsule position and fuel specimen linear power is given in Figure 3-3. The average linear power was 22 KW/ft with deviation of less than ±10 percent. The reactor experienced 19 scrams during the two-cycle irradiation. Pertinent irradiation data are summarized below:

B4A Irradiation

| Cycle Number | 48 | 49 | Total |
|---|---|---|---|
| Time, days | 22.3 | 26.9 | 49.2 |
| Linear power, Maximum KW/ft | 22.9 | 24.4 | 24.4 |
| Linear power, Minimum KW/ft | 20.9 | 20.0 | 20.0 |
| Linear power, Average KW/ft | 22.1 | 22.2 | 22.2 |
| Deviation percent | 9.1 | 19.8 | 19.8 |
| Burnup MWD/t | 6640 | 7920 | 14,560 |

3.3.1.3 Examination

Examination of this capsule was made difficult by the desire to observe short-lived activity in the fission gases and sodium. The difficulties represent precautions which must be taken as a result of the hazards of remote handling in the alpha enclosure of the capsule, sodium container, and fuel specimen, which were thermally hot and which contained large amounts of radioactive iodine, plutonium, NaK, and sodium. A well planned procedure to execute the examination was developed before the examination began. Nitrogen cooling equipment was used to control component surface temperatures during the various disassembly operations.

The capsule was taken into the RML on December 2, 1963, 16 hours after shutdown of GETR. The capsule surface temperature rise in air was noted and the assembly cut to a size suitable for entry into the alpha enclosure.

Gross gamma scans of the capsule were then performed to observe activity distribution in the capsule and identify any unusual activity concentrations. Multi-channel analyses of specific points of interest on the gross gamma scan were then performed. As shown in Figure 3-1, these scans provided a valuable description of the distribution of fission activity and Na-24 activity before the capsule was opened. The scans were repeated on December 6, 1963, after the initial fission gas and sodium samples had been taken.

Gamma peaks in the nonfuel sections were observed at 0.32, 0.78, 1.15, 1.33, 1.38, and 2.76 Mev which are attributed to Cr-51 or I-131, ZrNb-95, Co-60, and Na-24. The location of structural components and sodium within the capsule by this technique proved to be useful during the disassembly. Also the absence of fission product activity gave an early indication that significant migration had not occurred.

Activity spikes can be noted at the fuel pellet-to-pellet interfaces which is a phenomena recently noted only when scans are taken after a short decay time. Further scans will be made so the half life of this activity may be identified.

After the first series of gamma scans was completed, the capsule was placed in an alpha enclosure and disassembly commenced. As a precautionary measure the NaK cover gas space was punctured and the gases removed for analysis. Fission gas was found, indicating that the sodium container evidently had failed during the irradiation. The gas sample was removed into an in-cell fission gas apparatus.* A small aliquot was analyzed within 26 hours after the reactor shutdown. The Xe-133 to Xe-133m ratio in this sample after correction to $t_o$ was $4.1 \cdot 10^{-3}$ which when compared to the branching ratio of the isomers (corrected for absorption cross sections) results in the conclusion that these gases were delayed of the order of days before their release from the fuel pin.

*Since the gas samples would be too radioactive to sample by the normal out-of-cell techniques.

The presence of 9.1-hour Xe-135 could not be confirmed in this sample, providing further evidence that the gases had experienced a delay time which was effective in depositing the vast majority of significant fission product and daughter activity within the fuel pin or sodium container.

Without awaiting the analytical results described above, the fission gas puncture hole was enlarged and a NaK sample obtained which was found to contain no fission product activity. Thus, it was judged imperative to continue disassembly until a sodium sample could be analyzed before 20.8-hour I-133 could decay (if present) to an undetectable level. The sodium container was sealed as a precaution against an iodine release, and a second fission gas sample obtained which, when combined with the first sample, represents a total fission gas release of about 65 percent (a preliminary value which will be confirmed at a later date). The fission gas in the sodium container represented about 10 percent of the total and was found to be identical in composition to that above the NaK. Thus, it was now apparent that the delay time was within the fuel pin and vent and that the vent had performed effectively.

On December 4, the top of the sodium container was cut off and the sodium above the fuel pin was sampled. The sodium container was then sealed and set aside until such time when the uncooled sodium container could be handled in the alpha enclosure. Unfortunately, the sodium sample was later found to be atypical of sodium inside the container. At this point, the previously-described gamma scanning of December 6 occurred.

On December 13, the sealed sodium container with fuel pin inside was punctured and the gases from inside the fuel pin removed for analysis. The Xe-133 and Xe-133m present in this sample were roughly equivalent to what one would expect from decay of the total I-133 in the specimen.

After the gas sample was removed, the top of the sodium container was again opened and the fuel pin removed by gently heating the sodium. The sodium in the container was then dissolved in alcohol and sampled for radio-chemical analysis. Analysis of this solution is proceding at this time.

Fuel pin measurements and sectioning will be continued in an attempt to locate the daughter products of the gaseous fission products and thereby determine the effectiveness of the $UO_2$ blanket, as compared to the vent, as the delay mechanism. The location of iodine as well as detection of any sodium in the fuel will also be goals of the investigation.

### 3.3.2 Capsule B4B, Vented-Without-Blanket Fuel Pin

Fabrication of capsule B4B was delayed as a result of a failure of the sodium container during sodium filling. The container failure resulted in loss of the test specimen.

The capsule was returned to the plutonium fuel facility for fuel pin removal and inspection. Inspection of the fuel pin showed that the soft solder plugs were no longer in place in the fission gas vent holes, and that sodium had entered the fission product reservoir. Additional examination showed that the majority of the fuel pellets were broken and could not be reused. Breakage of the fuel pellets was attributed to pressures imposed upon the fuel clad by a tubing cutter during removal of the capsule.

A spare B4B fuel clad had previously been provided and a sufficient quantity of fuel pellets was available for reloading. The replacement fuel pin was loaded and welded during the quarter.

### 3.3.3 Capsule B4C, Defective Fuel Pin

Fabrication of capsule B4C has been completed, and irradiation will commence in GETR cycle 51, January 1964.

## 3.4 Fuel Operating Limits

A review of the operating power levels of the FCR fuel was undertaken to determine experimental information needed to understand and predict the steady-state properties of the fuel and clad in the FCR.

Of immediate interest was consideration of radial gap size on fuel thermal performance.

### 3.4.1 Gap Conductivity Experiment

This experiment has a twofold purpose: The first is to determine the effect of gap size on the thermal profile of the fuel, and the second is to develop experimental data on the possible use of large gaps for control of possible fuel volume changes.

Additional experimental data from this capsule will include the relationship of the $\int_0^{T_c} k d\theta$ to fission gas release and the possibility of steady-state fuel slumping.

The gap conductivity experiment (capsule B5A) has been designed to determine the gap conductivity of three different gap sizes that may exist in the FCR fuel. This fuel test will contain four different fuel sections as shown in Figure 3-4. The design test parameters are listed in Table III-1.

The relative differences in the fuel microstructure will be used to establish the fuel surface and fuel center temperatures in each fuel section. Out-of-pile grain growth data on the same batch of fuel will be determined to develop the time-temperature conditions for incipient equiaxed grain growth. One fuel section will have a 0.062-inch diameter W-W 26 percent Re thermocouple to provide an in-pile calibration of grain growth data. The test will operate for 40 hours, which is quite adequate to develop an equilibrium microstructure. An argon back-fill atmosphere will be used to duplicate more closely the conductivity of steady-state gap atmosphere; i.e., fission gas.

TABLE III-1

DESIGN PARAMETERS OF GAP CONDUCTIVITY CAPSULE B5A

| | Fuel Section | | | |
|---|---|---|---|---|
| | 1 | 2 | 3 | 4 |
| Power Level (KW/ft) | 23 ±1 | 23 ±1 | 23 ±1 | 23 ±1 |
| Linear Power Output (W/cm) | 755 | 755 | 755 | 755 |
| Surface Heat Flux (Btu/hr-ft$^2$) | $1.2 \times 10^6$ | $1.2 \times 10^6$ | $1.2 \times 10^6$ | $1.2 \times 10^6$ |
| Nominal Cold Diametral Gap (mils) | 4 | 2 | 10 | 4 |
| Back Fill Atmosphere[1] | A | A | A | A |
| Time In-Pile (hrs) | 40 | 40 | 40 | 40 |
| Clad OD (inch) | 0.252 | 0.250 | 0.258 | 0.252 |
| Clad ID (inch) | 0.222 | 0.220 | 0.228 | 0.222 |
| Center Thermocouple[2] | yes | no | no | no |
| $\int_{T_s}^{T_c} k d\theta$ (W/cm)[3] | 38.2[5] | 46.2 | 46.2 | 46.2 |
| $\int_{o}^{T_s} k d\theta$ ($T_s$ estimated) (W/cm)[4] | 45 | 39 | 55 | 45 |
| $\int_{o}^{T_c} k d\theta$ ($T_s$ estimated) (W/cm) | 83.2 | 85.2 | 101.2 | 91.2 |

(1) Argon is used as back-fill atmosphere to duplicate more closely the thermal conductivity of of fission gas.

(2) Thermocouple is W-26 percent Re clad W wire per Task E design (0.062-inch diameter).

(3) Using a power shape factor of 0.77.

(4) Using latest AECL $\int k d\theta$ curve for $UO_2$ (Journal of Nuclear Materials, Vol. 7, No. 3, 1962, p 225-262).

(5) Using power shape factor of 0.635 because of 0.062-inch hole for thermocouple.

Design of the experiment was completed and detailed design of the fuel pin and capsule was initiated. Approved drawings for this capsule and fuel are scheduled for completion in January 1964, and the capsule irradiation is tentatively scheduled for June 1964. The Form 21 for this experiment was transmitted to the AEC for approval on November 22, 1963.

### 3.4.2 High Power Tests

Under design is a series of three capsules designated B6A, B, and C, which will operate fuel specimens at power levels of 30, 35, and 40 KW/ft for 40 hours with clad temperatures near 1100 F. The purpose of these fuel tests will be to establish the upper operating power level of FCR fuel as defined by clad diameter increase caused by the presence of molten fuel. The fuel will be restrained in the axial direction to simulate the conditions expected in full length rods. The exact amount of molten fuel that will exist in these capsules is difficult to predict because of the lack of knowledge of the thermal conductivity of the mixed oxide. Assuming thermal conductivity of the mixed oxide to be the same as $UO_2$, the molten area of the fuel in these capsules will be approximately 15, 25, and 40 percent. Additional information will be determined by this experiment on the relationship of the $\int_0^{T_c} k d\theta$ to fission gas release, volume change and melting.

These tests are being designed to operate in the VB-4 Hydraulic Rabbit Facility at MTR which has a flux of $1.86 \times 10^{14}$ nv. The results of this experiment will be related to the 40-hour B5A experiment and to the out-of-pile grain growth experiments.

The experiments were designed and contact with MTR established to obtain the necessary design values for the facility. Preliminary designs of fuel and capsule were completed. Additional physics calculations necessary to set the enrichment level of these capsules are expected to be completed next quarter.

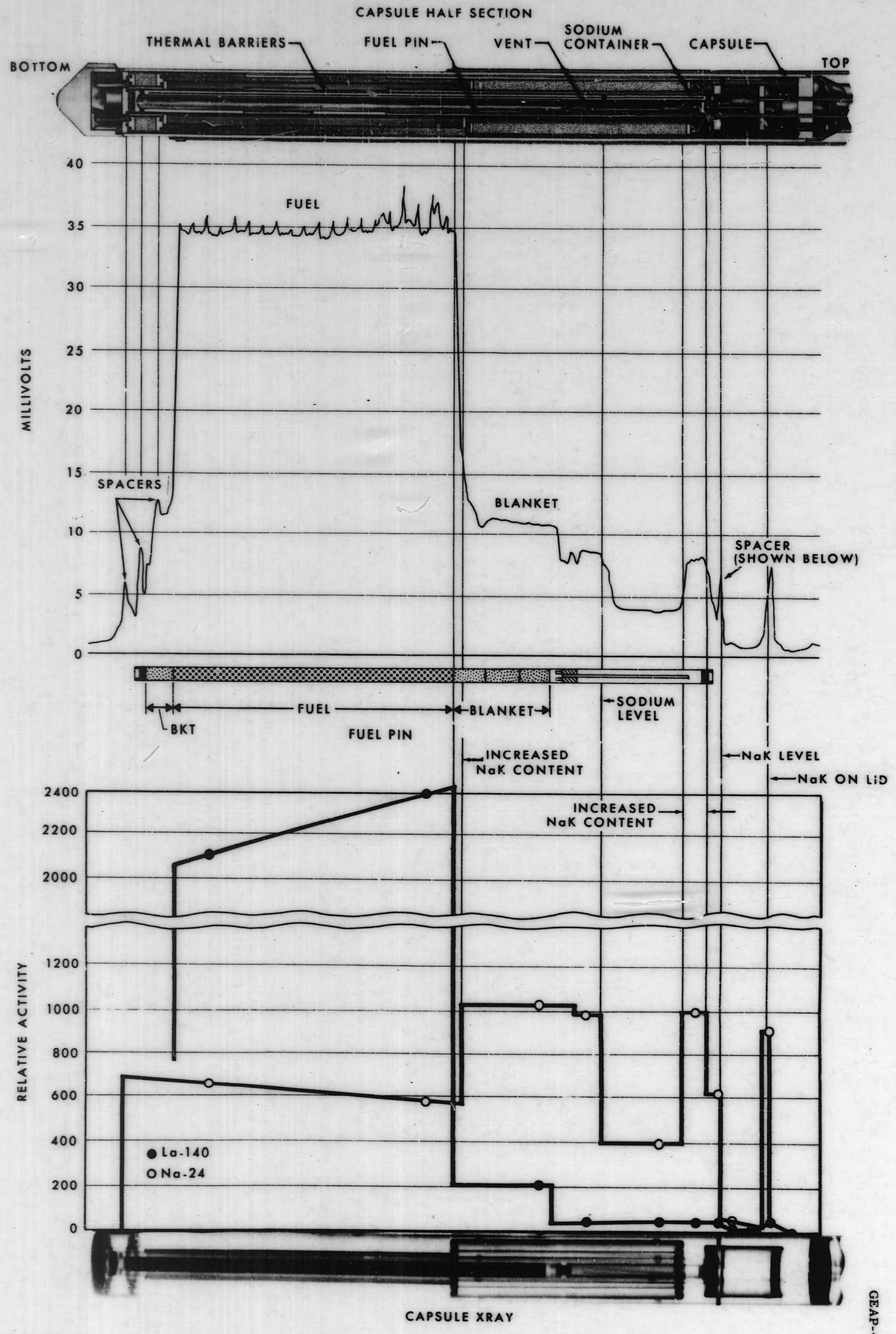


Figure 3-1. Isometric and Gamma Scan of Capsule B4A

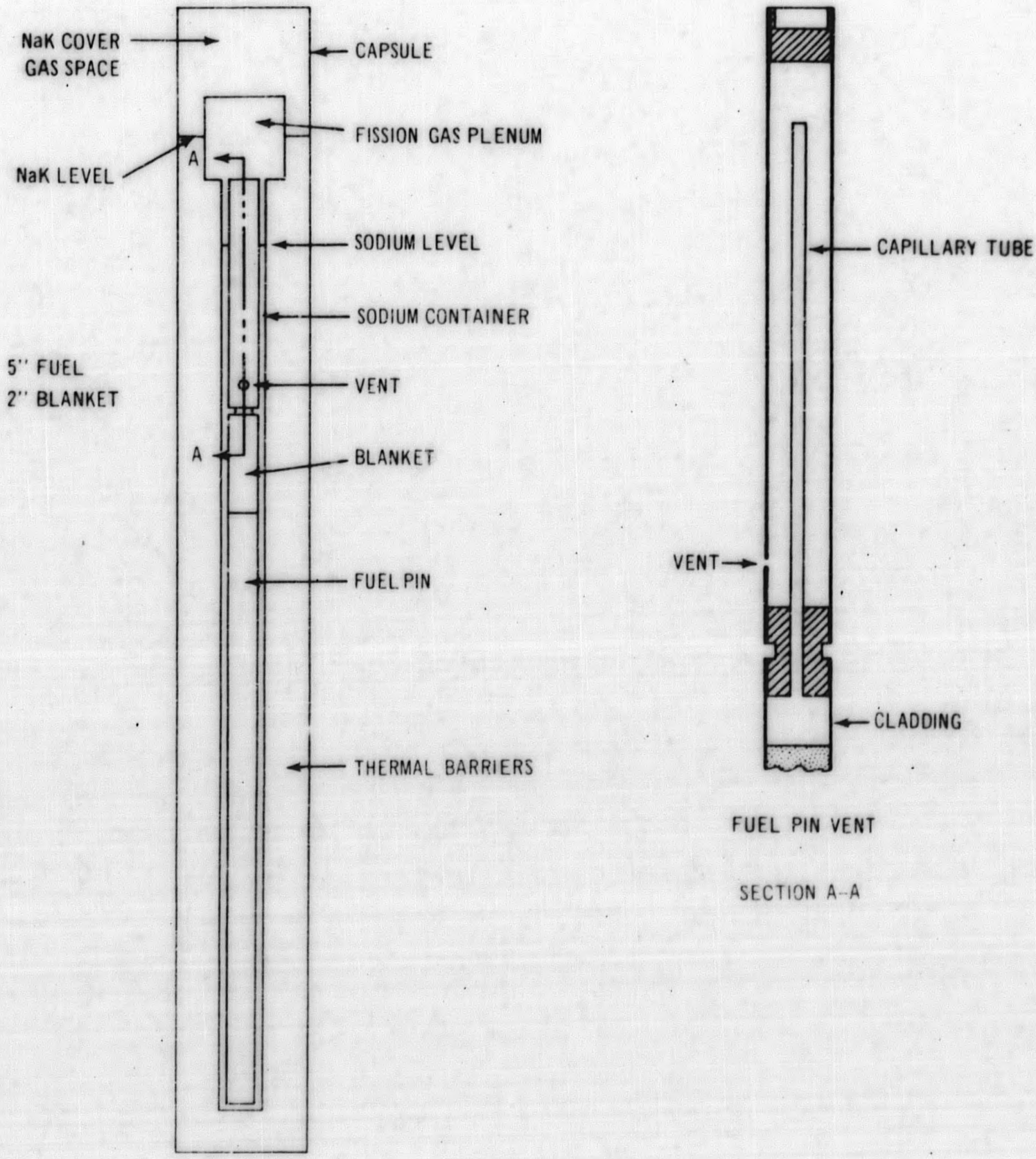


Figure 3-2. Schematic of Capsule B4A

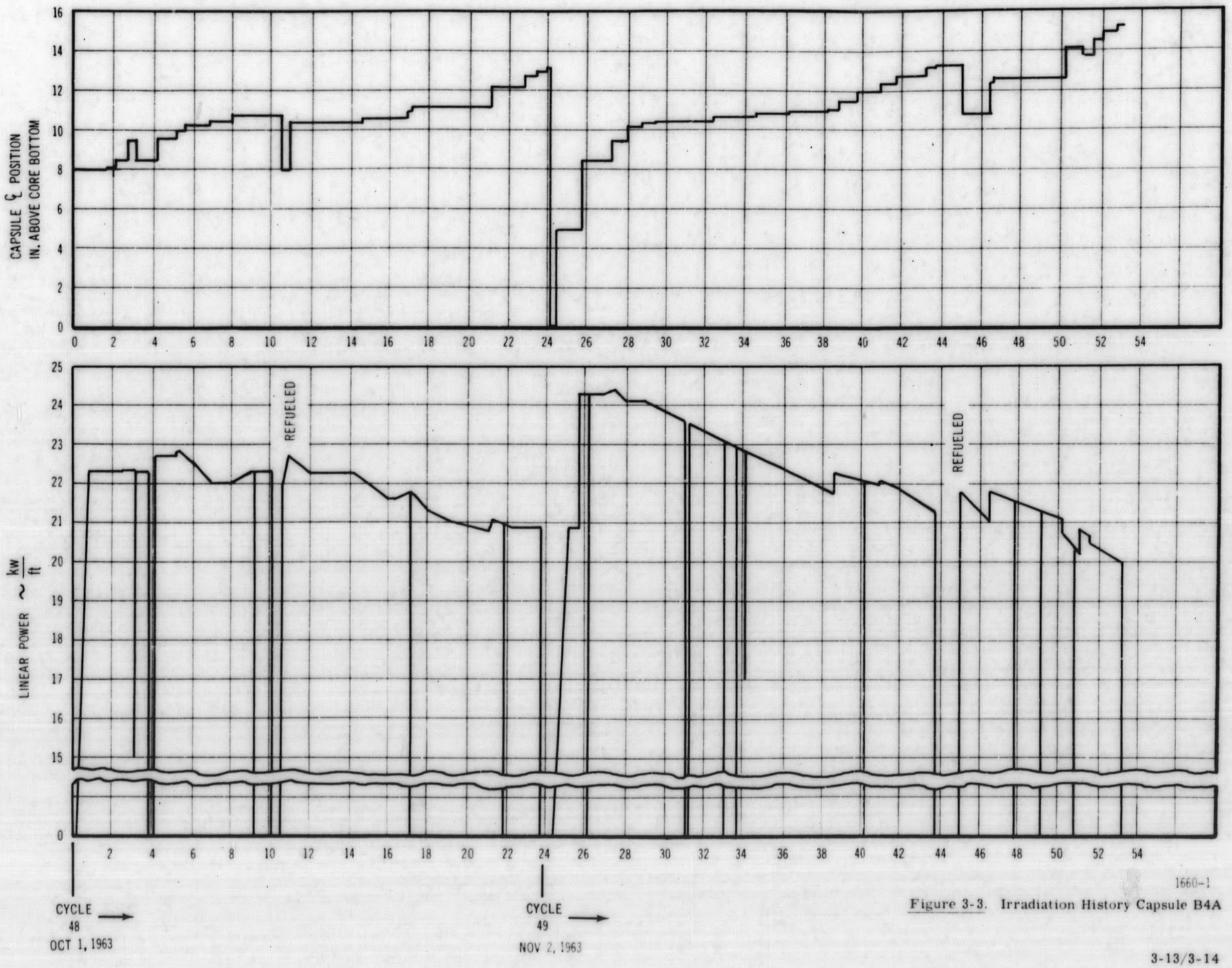


1660-1

Figure 3-3. Irradiation History Capsule B4A

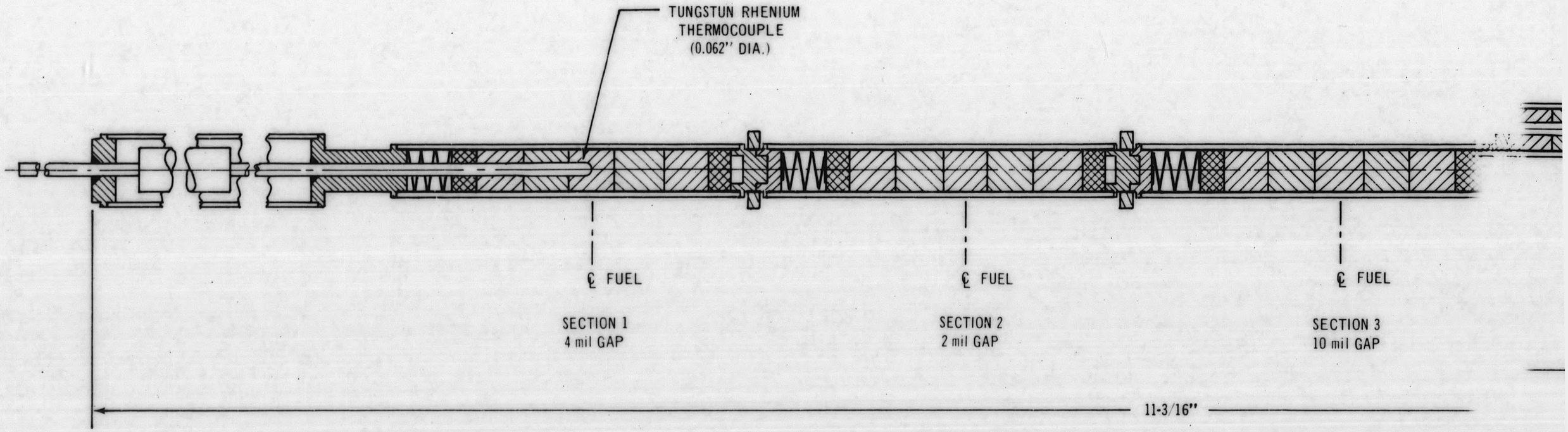
TUNGSTUN RHENIUM
THERMOCOUPLE
(0.062" DIA.)
℄ FUEL
℄ FUEL
℄ FUEL
SECTION 1
4 mil GAP
SECTION 2
2 mil GAP
SECTION 3
10 mil GAP
11-3/16"

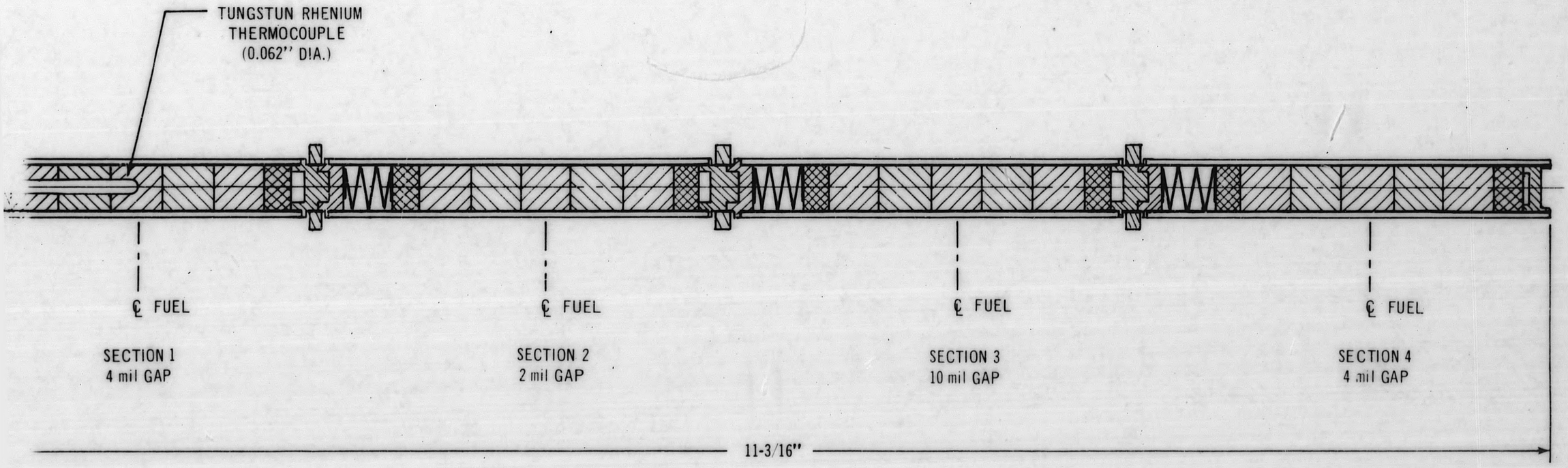


Figure 3-4. Fuel Sections - Capsule B5A

# SECTION IV

## TASK C - TRANSIENT TESTING OF FUEL

### 4.1 Series 2 - Unirradiated Mixed Oxide

This initial investigation of transient effects on 0.25 inch diameter mixed oxide fuel is now two-thirds complete. Tests completed to date on the initial sample, C2A, and on the second sample, C2B, have been described in GEAP-4300[1] and GEAP-4382[2] respectively.

#### 4.1.1 Specimen C2C

Requirements for the next test are based upon the need to identify the transient magnitude necessary to cause measurable increase in clad diameter. Estimated fuel vapor pressure relationships and calculated clad temperatures indicate that the clad yield strength could be exceeded with a peak fuel temperature only slightly in excess of 7000 F. The desired transient for the next test, therefore, is one which will result in a ~5 percent fuel temperature step ($\Delta T$ including heat of fusion) above the previous run.

Due to the rapid heat loss from the test sample and the relatively "slow" transients of this series, peak fuel temperature is apparently very sensitive to the power insertion curve shape. Transient definition, therefore, has required heat transfer computer calculations in which the input was varied until the desired peak temperature increase resulted. In accordance with advice from TREAT personnel,[3] calculations have been based upon integrated power data rather than the instantaneous power traces.

Figure 4-1 illustrates the transient curves desired for the next test as compared with the integrated power data from the previous run. The instantaneous power (Safety No. 1) from transient No. 581 is not shown since it did not agree with the integrator data. Calculated time of maximum fuel temperature is also shown, indicating that beyond this point the rate of energy insertion falls below the calculated heat dissipation rate. Based on previous data, the estimated reactor input parameters necessary to achieve this transient are 1.39 percent $\Delta K$ reactivity insertion resulting in a 1.29 second initial period (see Figure 4-2).

#### 4.1.2 Hazards Analysis

Series 2 tests are now approaching temperatures (7000 F) at which clad rupture can possibly be expected as a result of a high fuel vapor pressure combined with low clad strength. This occurrence could conceivably result in the introduction of extremely high temperature (liquid) fuel into the stagnant NaK coolant, creating a situation in which dynamic rather than static conditions might become significant to the hazards analysis. This section is a summary of the estimated capsule capabilities based upon some dynamic model assumptions.

4.1.2.1 Series 2 and 3 Inner Capsule Integrity

Capsule Model

The dynamic model used in this analysis was based upon the Series 2 and 3 TREAT capsule, as shown schematically in Figure 4-3. The fuel clad rupture was assumed to occur at the point where it could cause maximum damage, near the top of the fuel column, exposing molten fuel at ~7000 F to several cc's of liquid NaK at ~1000 F. The 6-inch long heat sink, located concentrically around the fuel, will tend to reduce the capsule wall pressure, except at either the top or bottom of the fuel. At these locations the vapor pressure will be transmitted directly to the capsule wall via the NaK coolant.

Figure 4-3 also illustrates the heater can wall, which will act as reinforcement after the capsule has expanded a few mils. This will allow the walls to experience a greater pressure before failure occurs. Also present, but not shown on the model diagram, is the third containment, which consists of the large 4-inch diameter can surrounding the heater can and capsule.

For the initial calculation it was assumed that following fuel expulsion, a NaK vapor film will form, followed by a rapid increase in NaK surface temperature until either a vapor pressure high enough to rupture the capsule was reached, or the fuel begins cooling, thus allowing the NaK temperature to level off and tend towards equilibrium. Since the attempt was to define the maximum limit (worst case), the model here assumed a constant heat flux "q" emitted from the fuel, across the gap and to the NaK. This treatment assumed a constant fuel temperature (7000 F) existing for a definite length of time, which physically could represent a continuous stream of fuel squirting into the NaK reservoir. By checking the various means of heat removal, it was found that conduction and convection could be neglected compared to radiation, at these high temperatures. The heat was thus transferred by radiation from the 7000 F fuel surface to a NaK surface that was initially at 1000 F. The time required to heat the NaK surface to a temperature (vapor press) high enough to cause capsule rupture, compared to the time duration the fuel could conceivably remain at a high constant temperature, determined the pressure pulse the capsule might experience.

Theoretical Approach

Solutions for the temperature change as a function of time, generally categorized as transient state heat transfer, have been worked out for many geometries and boundary conditions.[4] The situation involving a constant heat flux impinging on the surface of a flat plate was solved by Heisler[5] and used there, for surface and center temperature calculations of a plate exposed to induction heating. This approach satisfies very well our initial model (Figure 4-4), which employs a constant heat flux radiating to the surface of liquid NaK.

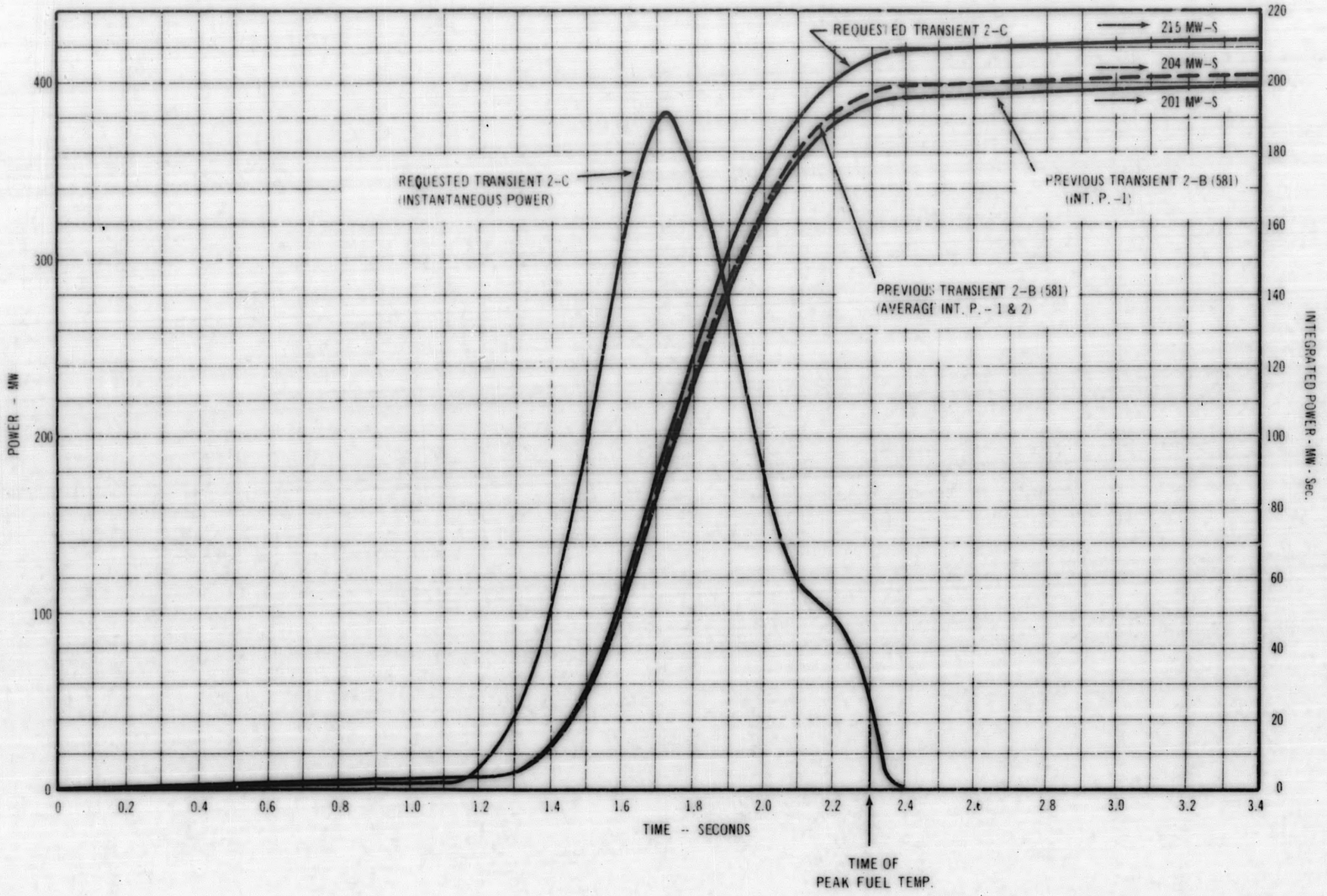


Figure 4-1. Previous Transient 2-B(581) and the Requested Transient for Capsule 2-C

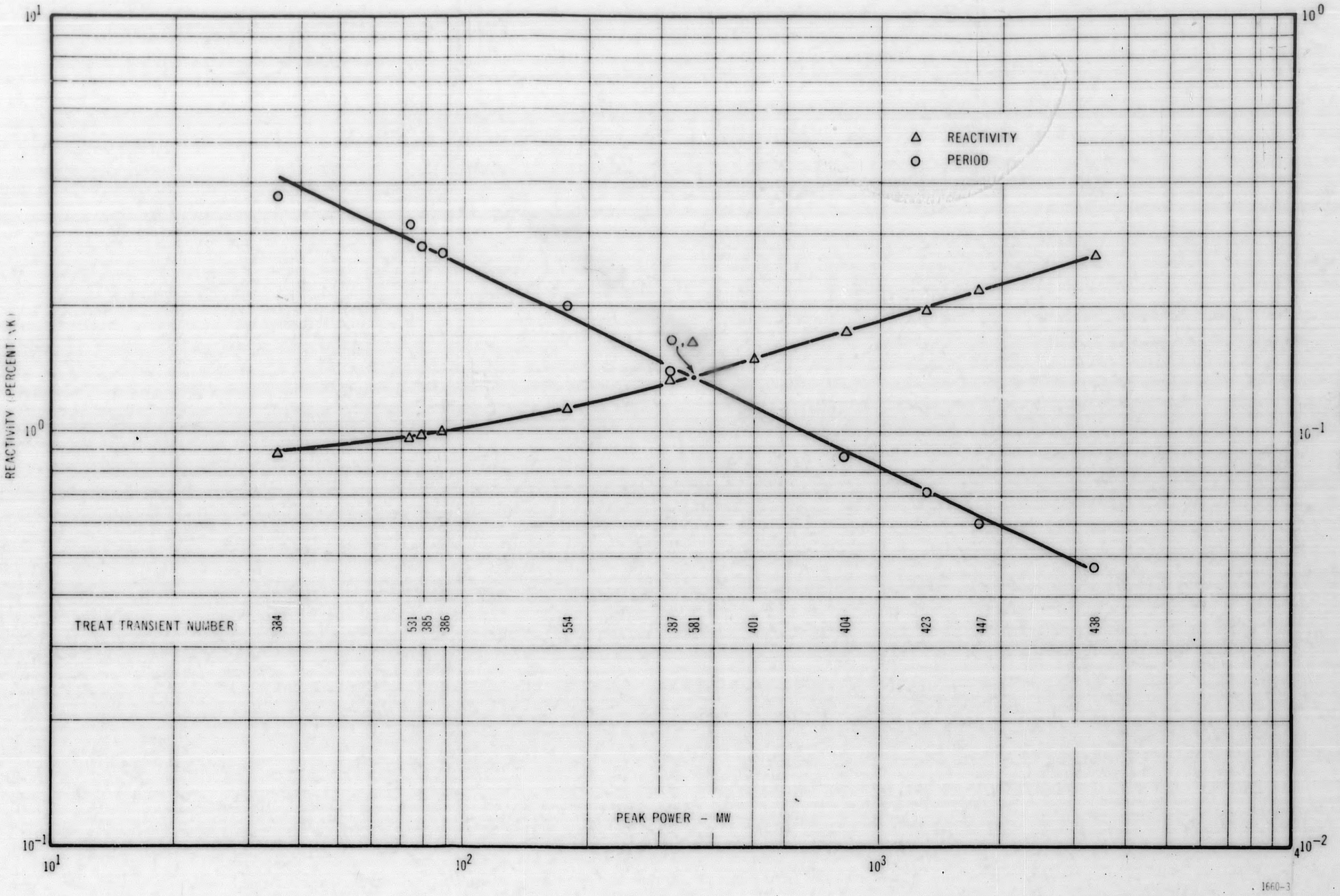


Figure 4-2. Measured Values of Reactivity and Reactor Period as a Function of Peak Power for Various Treat Irradiations

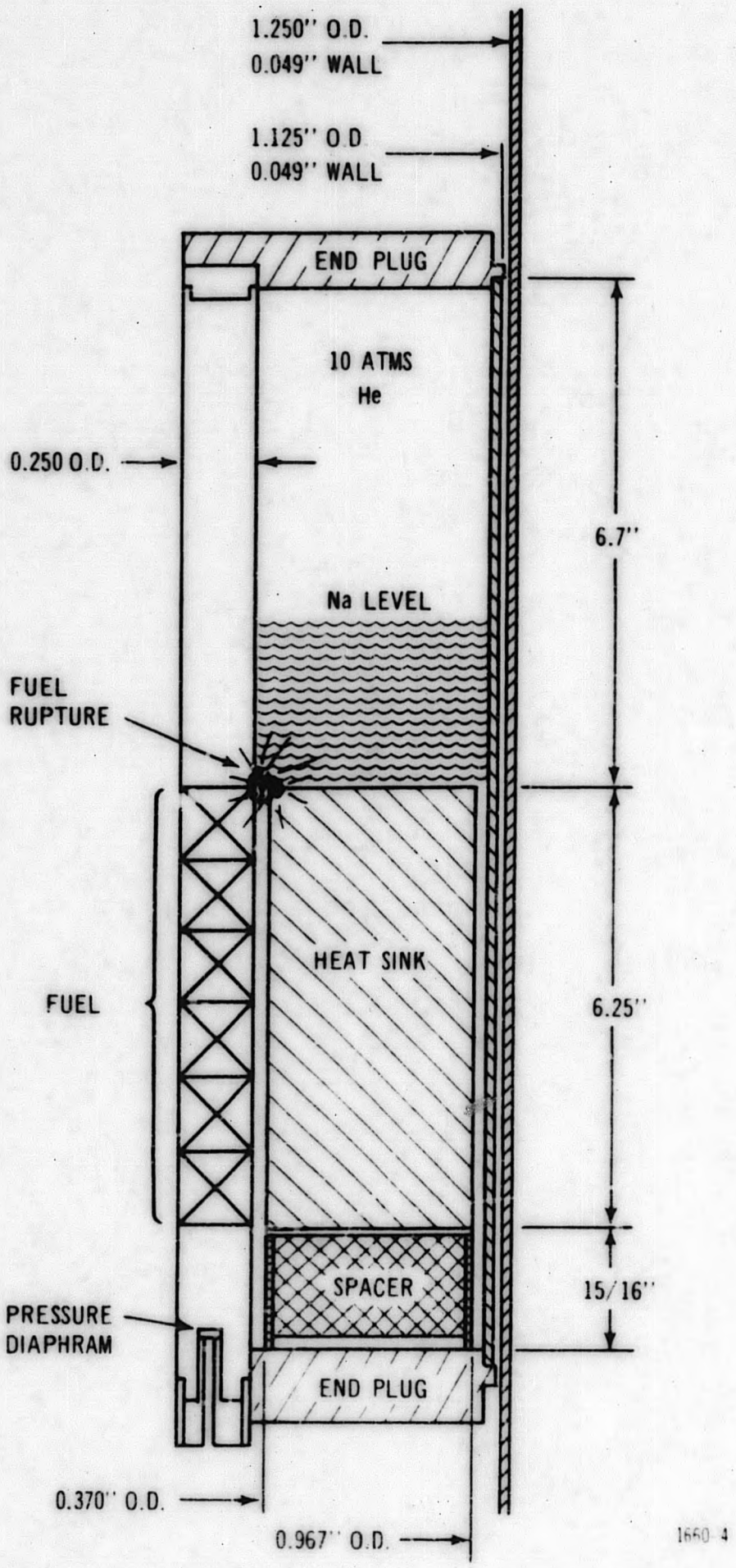


Figure 4-3. Capsule Model

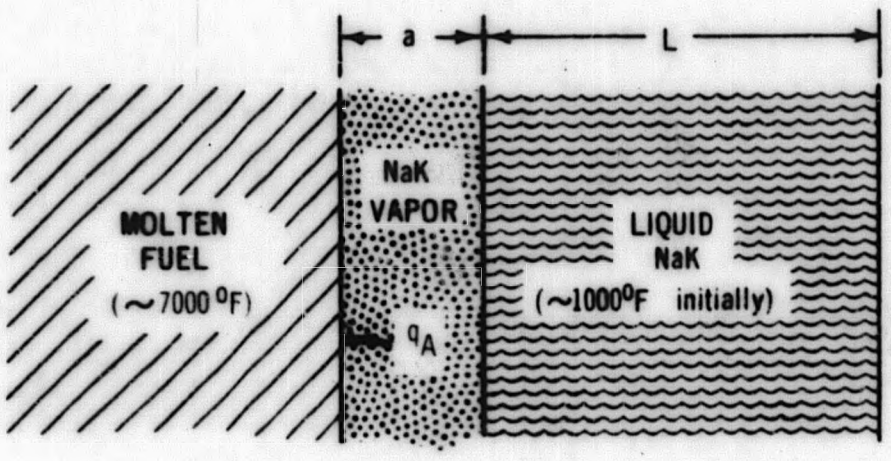


Figure 4-4. Initial Model

The dimensionless graphs illustrated in Heisler's report permitted a rapid calculation of the NaK surface temperature as a function of time, after exposure to a given heat flux. The NaK (plate) thickness "L", and heat loss are accounted for in the dimensionless formula for each specific case. From this surface temperature, the vapor pressure of the NaK at any instant in time was found. By selecting the proper dimensions and properties for the model, it was possible to construct a plot of estimated pressure and temperature vs. time.

Thus, in the case considered, it can be seen from Figure 4-5 that to produce vapor pressures approaching capsule static limits, would require exposure of 7000 F fuel to the NaK for at least 0.7 seconds. This situation is very unlikely since even the peak fuel temperature in the accident case (110 percent of the requested value) remains above 7000 F for less than 0.8 seconds.

4.1.2.2 Supplementary Factors

Section 4.1.2.1 covered hazards calculations for an assumed model based upon fuel clad penetration in the Series 2 capsule. In this case, as the analysis was simplified to allow ready computation, the more pessimistic assumptions were utilized. Several areas of further refinement exist, therefore, and are briefly defined in this section. These areas have not been pursued in detail, but are presented as a qualitative indication of the safety factors involved in the requested transient test.

1. NaK Vapor Gap as an Insulator

   The original dynamic model assumed the NaK vapor gap to be transparent to infrared radiation, thus having no effect on the radiative heat transfer to the bulk liquid NaK. This, no doubt, is a pessimistic assumption, although a value for the transmissibility of NaK vapor is not readily available. In the actual situation, the vapor gap probably acts as an insulator, decreasing the rate of heat transfer and the ensuing rise in NaK vapor pressure.

2. Fuel Not an Infinite Heat Source

The assumption of an infinite heat source at a constant 7000 F is probably more severe than will be experienced. Immediately after the fuel is forced from the pin, bubbling and mixing should occur, causing rapid cooling of the fuel and possibly sealing the leak. The actual mechanisms involved here are purely speculative and difficult to reasonably analyze theoretically.

3. NaK Movement

The question has arisen as to whether NaK movement will occur, relieving any dynamic vapor pressure, before the effects are felt by the capsule wall. As the liquid NaK surface rises in temperature, the pressure increases gradually, providing time and the driving force necessary to move the liquid NaK upward. This movement should reduce or stabilize the pressure in the moving NaK as the vapor gap becomes larger. However, there may still be pockets of NaK off to the side or underneath the vapor void which cannot move, thus remaining in direct view of the hot fuel. These pockets can continue to develop very high local vapor pressures which may be transmitted to the wall by methods similar to the model already used. This would seem to indicate that the dynamic load as calculated before is not necessarily relieved by NaK movement, but instead, represents a "worst case" situation.

4. Inner Capsule Wall Reinforcement

In all calculations of Section A the ultimate strength of the inner capsule wall determined the failure limit. In the actual case, however, the inner capsule is surrounded by a heater can such that a reinforced capsule model resembles more closely the actual situation occurring during deformation. Only a small expansion (0.013 inch radially) of the capsule is necessary before it receives additional resistance from contact with the heater can wall (1.152 inch ID 0.049 inch wall). This reinforced capsule will then act as a single wall 0.098 inch thick, and was treated as such in the following calculations. Capsule failure is still assumed to occur at a deflection of 50 percent, but the allowable dynamic load is much greater than in the case of the capsule wall unreinforced. Initial static conditions for the reinforced capsule are:

$$P = \frac{2\sigma t}{d} = \frac{2\,(0.098)\,\sigma}{1.152}$$

$$= 0.170\,\sigma$$

at 800 F

| | | |
|---|---|---|
| $P_y$ | 0.170 (21.500) | 3660 psi |
| $P_b$ | 0.170 (62.500) | 10.620 psi |

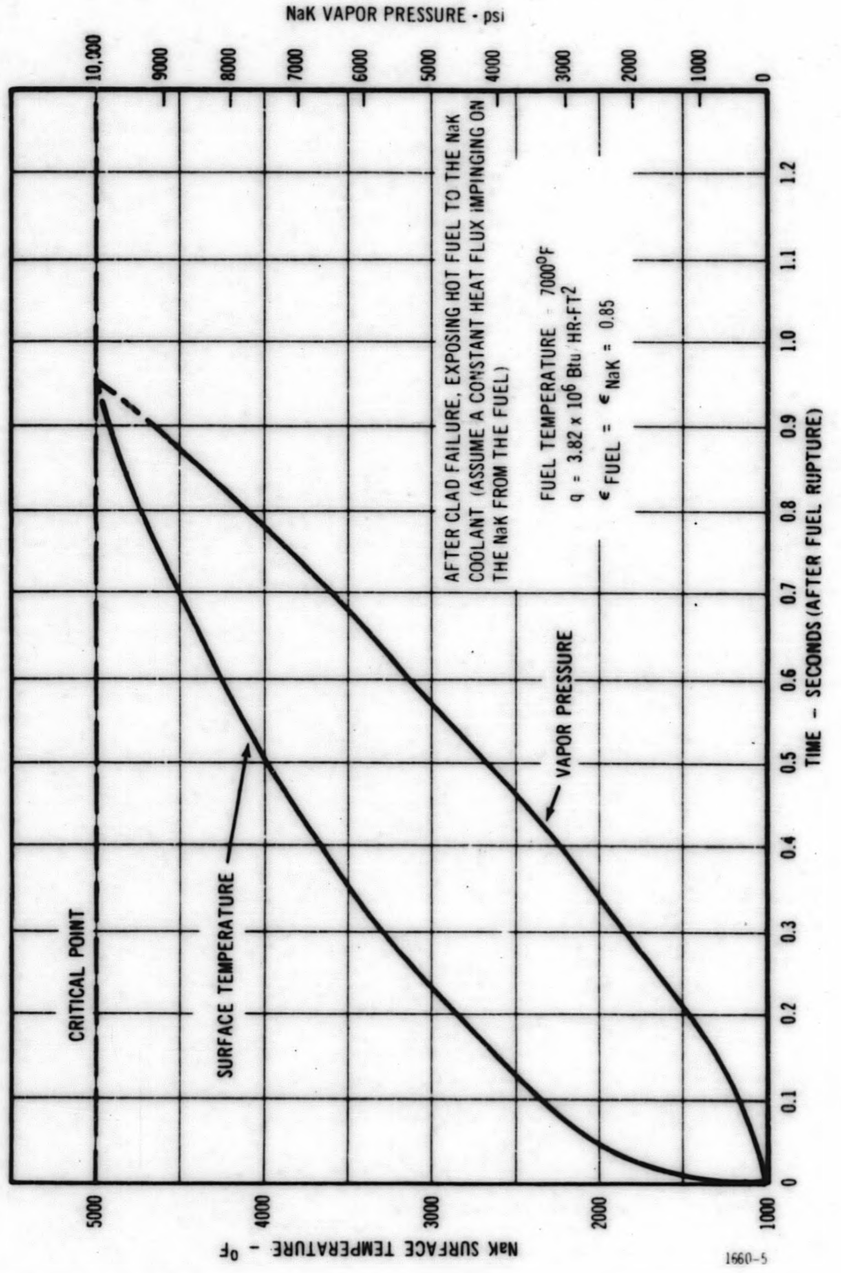


Figure 4-5. NaK Surface Temperature and NaK Vapor Pressure vs. Time

5. Effect of Heat Sink on Capsule Strength

If the fuel rupture occurs near the axial center of the fuel pin, the capsule walls will be effectively shielded from the immediate pressure pulse by the aluminum heat sink. This heat sink would have to expand 0.079 inch radially before capsule deformation would begin to occur. Since the heat sink is thick (~0.300 inch) it will offer considerable resistance to the pulse, and probably force the maximum deformation elsewhere (either axially or above the heat sink). A detailed analysis of this case has not been completed since it cannot be assumed that the fuel rupture will always be within the area surrounded by the heat sink.

6. NaK Emissivity

In calculating the radiative heat transfer in the first model, the value of $\epsilon = 0.85$ was assumed for the NaK surface. This value assumes a severely contaminated, oxidized surface and could be too high by a factor of 10 ($\epsilon = 0.06$ for a smooth, shiny surface). Although it is difficult to guess the exact condition of the surface, it is significant to note that halving the assumed value of $\epsilon$ would result in a factor of four increase in the time required to reach the critical temperature.

7. Dynamic Loading

It should be noted that in the previous calculations, the static ultimate strength was used to determine the inner capsule failure point. If, however, the pressure pulse is more rapid than calculated, a dynamic loading situation may result in which considerably higher, instantaneous stresses can be withstood. Calculations using the method described in reference 10, however, indicate that extremely short pulses (~0.1 msec) are necessary before appreciably higher strengths can be assumed.

4.1.2.3 Outer Can Integrity

A recommended continuation of the previous inner capsule analysis involved increasing our knowledge of the outer can capabilities, more specifically, a determination of the effects of shock loading and missile penetration. This analysis is now completed and the results summarized herein.

1. Missile Penetration

If the inner capsule is exposed to pressure bursts greater in magnitude and duration to those stated previously, the possibility of capsule rupture exists. Although the capsule wall will remain ductile and should not shatter, some stainless steel fragments might tear loose and impinge on the heater can or outer capsule. The velocity, size and shape of these fragments determines their penetrating ability, thus giving an indication of outer capsule integrity.

a. Probable Fragment Velocity

The maximum capsule wall velocity at the time of rupture can be deduced from the equations used in an earlier analysis. This value will be used as the initial velocity of any fragment.

The wall velocity can be derived from the following equation.[6]

$$\frac{dr}{dt} = \left[ \frac{2}{\gamma\, h_o r_o} \left\{ \frac{P_d}{2} (r^2 - r_o^2) - \frac{2 r_o \sigma_o h_o}{3} \left[ \ln r - \ln r_o + \frac{H}{3} \left( \ln \frac{r}{r_o} \right)^2 \right] \right\} \right]^{1/2} \qquad (1)$$

The maximum velocity was obtained by assuming a step pulse of 15,000 psi continuing until failure. This value for pressure represents a "worst case" as it is equal to the vapor pressure of NaK at the assumed fuel temperature of 7,000 F. Substituting the appropriate values into equation 1, yielded an initial fragment velocity of 1155 ft/sec (wall velocity at rupture).

b. Particle Size and Energy

The determination of fragment dimensions and energy necessary to penetrate various wall thicknesses was accomplished by using empirical data[7] for mild steel. It has been found experimentally that maximum penetration occurs with fragments in the form of long rods and requires a penetration energy given by the following formula:

$$e = 16{,}000\, T^2 + 1{,}500\, T = \frac{1}{2} \frac{W V^2}{g d}$$

where

e = kinetic energy per unit diameter of rod (foot-pounds per inch)
T = wall thickness (inches)

With the penetration energy and fragment velocity known, the required rod size can be determined, assuming the rod diameter equal to the capsule wall thickness. This resulted in a calculated minimum fragment length of 0.865 inch.

Not only is the formation of a fragment of this size unlikely, but it must strike the target wall endwise to penetrate under these conditions. This means the rod must turn ~90 degrees before contact, which is virtually impossible in the available space (~0.060 inch between capsule and heater can wall). Only if the heater can inner wall were already ruptured would the rod have the necessary space needed to

turn perpendicular before striking. It should be pointed out, however, that in any case there is additional containment since the fragment must penetrate 1/2 inch thermoflex and a 0.060 inch heater can wall, followed by the 0.065 inch outer capsule wall. Since the calculations above indicate that a 0.050 inch wall is sufficient to stop any fragments, the missile penetration seems negligible as a hazard.

2. Shock Pressures

Although it is improbable that the inner capsule will fail explosively, an analysis was made assuming such a failure, producing shocks which propagate to the heater can and outer capsule walls. The shock model assumed that 15,000 psi helium from the inner capsule was instantaneously brought in contact with the atmospheric helium in the outer can (Figure 4-6).

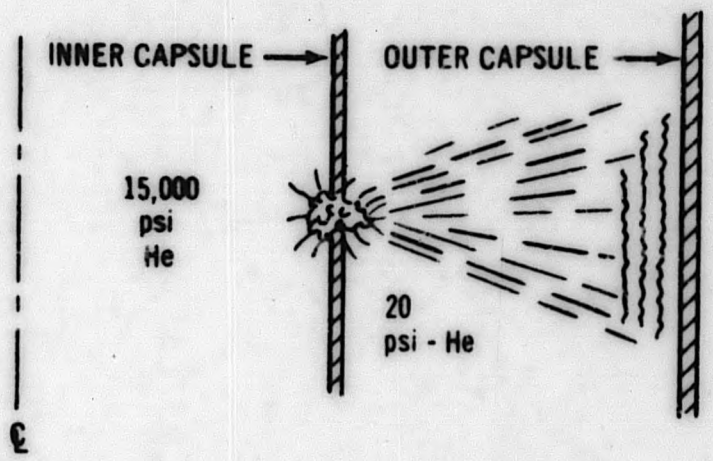


Figure 4-6. Shock Pressures

This model will generate shock waves in the atmospheric He which quickly propagate to the outer wall causing dynamic pressures much smaller than the driver gas (15,000 psi), but higher than the initial outer can pressure. This situation is similar to that in a shock tube[8] and appropriate shock theory may be used. The pressure profile experienced by the outer capsule wall is shown in Figure 4-7.

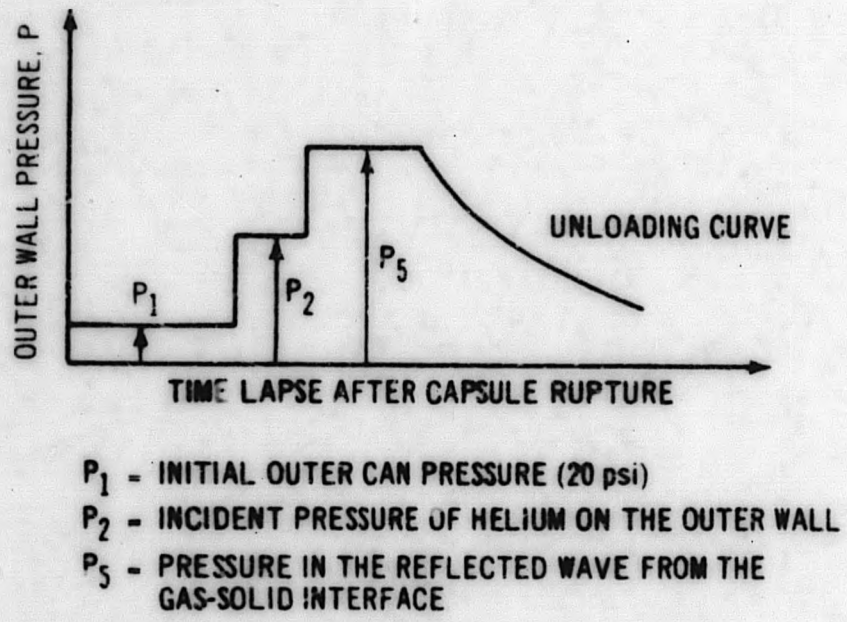


Figure 4-7. Pressure Profile

At some time $t > 0$ the capsule ruptures, allowing 15,000 psi helium to contact static helium at 20 psi ($P_1$). This produces a shock wave which proceeds towards the outer capsule wall at pressure $P_2$. The shock wave is reflected with a higher pressure $P_5$, and is directed back towards the inner capsule. All reflected pressures after $P_5$ will be neglected since their values are less than $P_5$.

Using the appropriate relationships from reference 8, it was calculated that $P_5$ would not exceed 1070 psi. This is the maximum dynamic shock pressure that the capsule wall experiences after an explosive release of 15,000 psi from the inner capsule. Comparing this pressure with the static capabilities of the outer can:

since $d/t = \frac{4.00}{0.065} \gg 10$, we will use thin wall analysis:

yield strength, $P_y = \frac{2\sigma_y t}{d} = \frac{2\ (40,000)\ (0.065\ \text{inch})}{4.00\ \text{inch}}$ (304 SS at 200 F)

$$= \underline{\underline{1,300\ \text{psi}}}$$

burst strength, $P_b = \frac{2\ (69,000)\ (0.005\ \text{inch})}{4.00\ \text{inch}}$

$$= \underline{\underline{2,240\ \text{psi}}}$$

It is seen that the shock pressure generated is less than the static yield pressure. Since the shock tube theory applied to this situation gives results which are pessimistic (i. e., the shock from capsule rupture will be dispersed over a larger surface area than the theory assumes, developing lower pressure per unit area), there is a considerable safety margin apparent.

## 4.2 Series 3 - Pre-Irradiated Mixed Oxide

This series of transient tests using 0.25-inch diameter prototypical FCR samples will represent the closest approximation to FCR conditions achieved to date. Pre-irradiation will include low burnup to form a central void and high burnup to generate substantial fission gas pressures.

### 4.2.1 Specimen C3A

This control sample was irradiated to ~7500 MWD/T in the GETR pool and examined to establish the condition of the sample prior to transient exposure. Details of the examination were previously reported in the preceding quarterly report.[2]

### 4.2.2 Specimen C3B

Reencapsulation of this first pre-irradiated transient experiment is imminent. Fabrication and assembly of parts has been completed for remote installation of the pressure transducer. Holding fixtures for the capsule and transducer are ready and a method for leak testing the welds has been developed. A practice installation has been performed using the unirradiated capsule C2C. Tentative plans for TREAT irradiation are to duplicate the C2B transient in which the peak fuel temperature reached ~6500 F. This target may be raised depending upon the possible results of the C2C irradiation.

### 4.2.3 Specimens C3C, C3D, and C3E

Capsules containing these samples remain under irradiation in the Z-10, Z-12, and X-5 pool positions (respectively) of the GETR. A total of nearly seven GETR cycles have now been completed (44 through 50) without loss of instrumentation. At the end of cycle 49 (December 1, 1963) the estimated burnup for the three samples, based upon thermocouple measurements was 37,300 (C3C), 38,700 (C3D), and 34,200 (C3E) MWD/T.

## 4.3 Series 4 - Transient Clad Rupture or Penetration

Preliminary conceptual design of a test capsule for this series has been delineated and specific heat transfer and physics calculations have been initiated. The capsule will be designed for low burnup pre-irradiation (~5000 MWD/T) prior to transient irradiation to the point of clad failure. Pressure containment and calorimetry will be two essential features of the TREAT capsule, with the fuel pin immersed in sodium in a geometry similar to that expected in a typical FCR core. The initial capsule will be primarily for calibration and will include a fuel thermocouple to provide correlation of TREAT power to peak sample fuel temperature.

# SECTION V

## TASK E - FUEL PERFORMANCE EVALUATION

### 5.1 Central Temperature Measurement of Mixed Oxide Capsule E1A

Irradiation capsule E1A containing a mixed oxide fuel pin and an all-urania fuel pin has been described in GEAP-4300.[1] Completion of the capsule fabrication and irradiation has been delayed due to defective thermocouples. The experiment is now scheduled to be irradiated in the GETR cycle 56 (April).

#### 5.1.1 Fuel and Capsule Fabrication

The fuel with a 100 mil central hole has been made and the capsule components have been fabricated.

#### 5.1.2 Fuel Central Temperature Thermocouple

The thermocouples to be placed in the central void of the fuel were received and an attempt was made to calibrate their emf characteristics. The test setup consisted of a small tungsten cylinder, induction heated, with a hole drilled in it to receive the thermocouple. The thermocouple to be calibrated was inserted into the axial hole to a predetermined length. Surface temperature of the thermocouple was determined by sighting into the other end of the hole with a disappearing-filament optical pyrometer.

During the course of the calibration it became apparent that external ground loops were disturbing the emf measured. The ground loops were eliminated and the test continued. Final results indicated that the thermocouples produced sub-standard and erratic emf. One of the thermocouples was destructively examined and found to contain impurities deposited on the insulator. X-ray diffraction and fluorescence identified the impurities as oxides of tungsten and rhenium. An attempt was made to clean up these oxides by reducing in hydrogen at 800 F. Neither this treatment nor soaking the thermocouple at high temperature in vacuum was adequate to correct the sub-standard emf. As a result, these thermocouples could not be used in completion of capsule E1A.

The previous thermocouple design consisted of a 20 mil wire centrally located within a 0.090 inch diameter sheath of tungsten - 26 percent rhenium by a concentric beryllia insulator for its entire length except for the last 3/4 inch at the hot junction where it is unsupported. This design has now been modified to a two-wire construction to eliminate ground loop currents.

## 5.2 High Burnup Irradiations

Two capsules are currently undergoing irradiation, each containing a sub-stoichiometric and a super-stoichiometric mixed oxide fuel pin. These capsules are periodically repositioned within the GETR pool to maintain a uniform axial flux shape along the fuel during the irradiation cycle. Thermocouples located within the capsule provide for positive determination of power generation rates at any point in time. These well-characterized, relatively long, (8 and 10 inches long) fuel samples will be irradiated to peak burnup of approximately 100,000 MWD/T. The capsule and fuel design is described in GEAP-4300.[1]

### 5.2.1 Accelerated High Burnup Capsule, E2B

As of the end of this quarter, capsule E2B has accumulated a peak burnup in the fuel of 30,000 MWD/2000 lb Pu+U. (See Table V-1.) During three cycles of irradiation the capsule has not received the specified neutron flux due to occasional sticking of the horizontal drive portion of the V-RAFT (Vertical and Radially Adjustable Facility Tube) mechanism. Target conditions have not been exceeded at any time, and axial power shape has been maintained at all times. The malfunctioning of the horizontal drive mechanism is being investigated and will be corrected.

TABLE V-1

LONG BURNUP CAPSULE E2B IRRADIATION LEVELS

| | | MWD/2000 lb Pu + U | | | |
|---|---|---|---|---|---|
| | | Cycle 48 | Cycle 49 | Cycle 50 | Total |
| E-2-B-1 | Peak | 11,350 | 8,370 | 10,400 | 30,120 |
| | Min. | 7,600 | 5,915 | 7,700 | 21,215 |
| | Mean | 9,500 | 7,140 | 9,050 | 25,690 |
| E-2-B-2 | Peak | 11,350 | 8,370 | 10,400 | 30,120 |
| | Min. | 6,500 | 5,000 | 6,400 | 17,900 |
| | Mean | 8,900 | 6,700 | 8,400 | 24,000 |

Thermocuples in the capsule are functioning properly. Local and total power indications of the eight thermocouples in the thermal barriers are internally consistent to within 7 percent. During the first cycle of irradiation in October (Cycle 48) the V-RAFT operated satisfactorily to maintain the specified peak flux within approximately ·5 percent. Figure 5-1 indicates the maximum and minimum temperatures recorded during each day of the cycle, these temperatures being proportional to the local heat generation within the fuel. The corresponding vertical and radial adjustments are also indicated. With increased attention to the specified limits it is expected that maximum power can be held to within ·3 percent. Figure 5-2 indicates the degree of correlation between the three methods of determining or measuring peak capsule heat-generation rate. The thermocouples in the thermal barriers (along with the calculated impedence in the heat

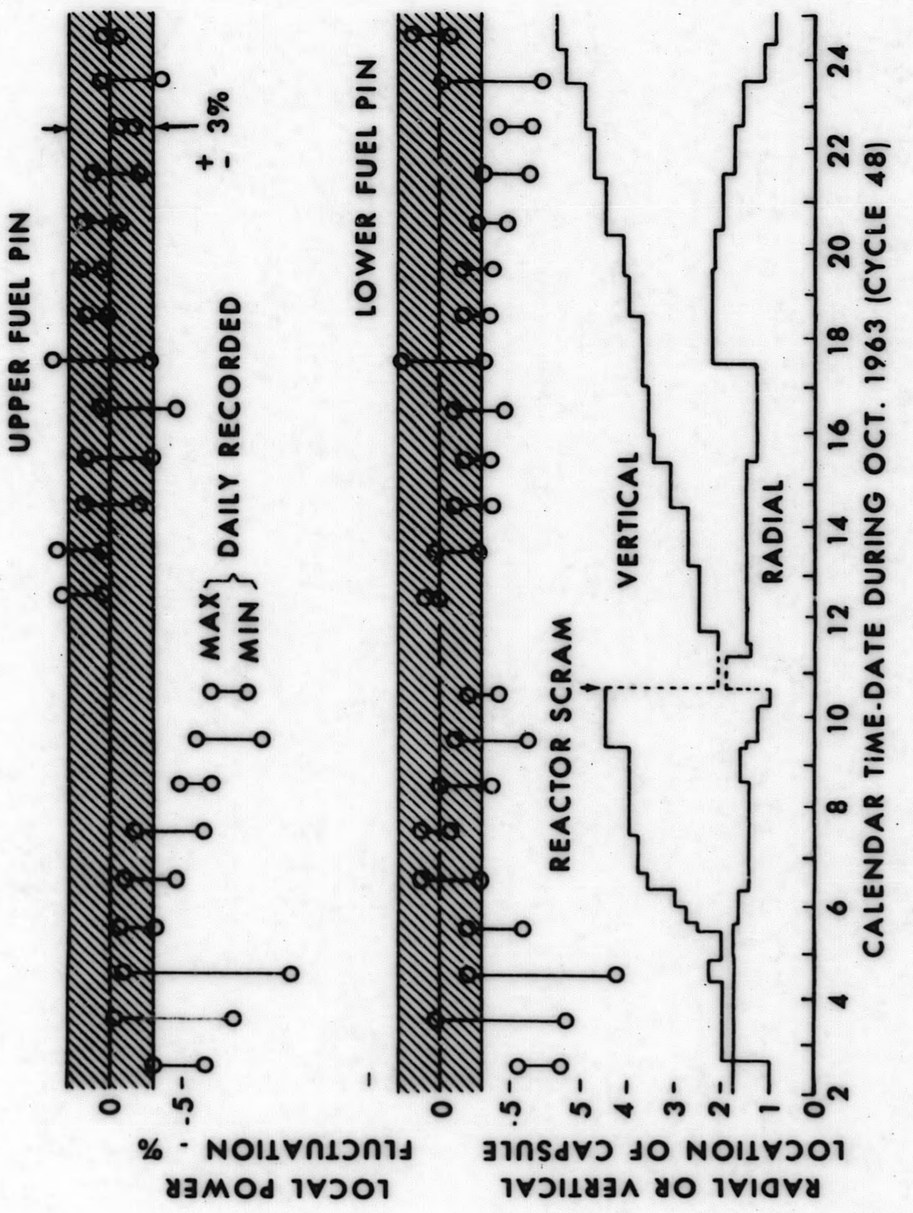


Figure 5-1. One Cycle Power Record

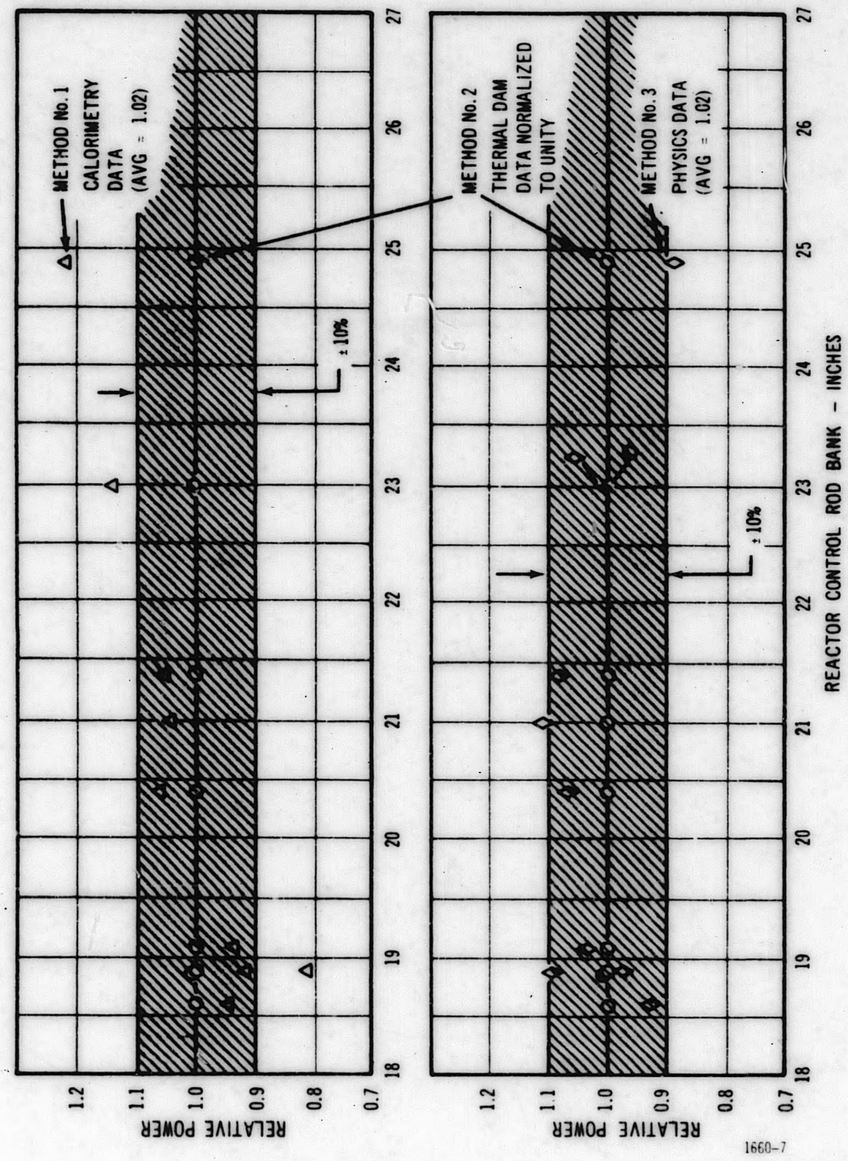


Figure 5-2. Peak Linear Power - Data Comparison Capsule E2B

transfer path between the two thermocouples) provide one method of local power measurement. The peak power generation rate determined by calorimetry is compared in the top part of Figure 5-2 as a function of time during the test reactor cycle as the control rods are withdrawn. Test data taken at different times during the cycle indicates an approximate range of ±10 percent for the correlation between the thermal dam power and the calorimetry power. The position of the capsule is known from operating records; hence, with known GETR pool fluxes the power in the fuel pin may be calculated based on the fuel cross sections. In the lower part of Figure 5-2 a comparison between the physics calculation and the thermal dam power also shows an agreement within ±10 percent on at any given point in time. Generally when averaged over an entire cycle, agreement between all three methods of power calculation or determination is within a very few percent.

### 5.2.2 Normal Power High Burnup Capsule E2A

Capsule E2A is identical to capsule E2B except for the larger diameter fuel (0.220 inch OD) of reference FCR conditions. Irradiation of this capsule started early in December. A repair of a cover gas leakage around a capsule thermocouple penetration was effected by brazing prior to the beginning of irradiation. During the first few hours of irradiation at a low power level some of the temperatures within the capsule were anomalous and higher than predicted. It was concluded that this was probably due to a lack of NaK bonding within certain regions of the capsule contrary to the design conditions. During one of the final stages of repair of the cover gas leak the capsule was inverted, making possible entrapment of some of the argon cover gas in such a way that the NaK could not properly flow into position. The capsule was withdrawn from the reactor flux on the V-RAFT and gradually brought up in power. Capsule temperatures gradually returned to normal after three days. One week later a low power condition developed over a period of an hour as indicated by the thermocouples for the lower pin within the capsule. The total power measurement from the capsule is normal and the anomalous thermocouple behavior has not yet been explained. Irradiation is continuing at reduced peak power (about 85 percent).

## 5.3 Plutonium Migration

### 5.3.1 Capsule Design

Design of capsule E3A is complete and an assembly drawing is shown in Figure 5-3. The six high temperature fuel specimens are surrounded by Zircaloy-2 and aluminum thermal barriers bonded with NaK. The entire capsule will be moved in the reactor flux to hold these six specimens at essentially constant power conditions and fuel surface temperatures of 1250 F. Two additional pins are located at the upper end of the capsule. These two pins will provide control data on self shielding and spatial distribution of isotopic composition needed for the interpretation of the high temperature experiments. These specimens are held at low temperature by placing them in a lower neutron flux and by surrounding them with NaK bonded aluminum thermal barriers.

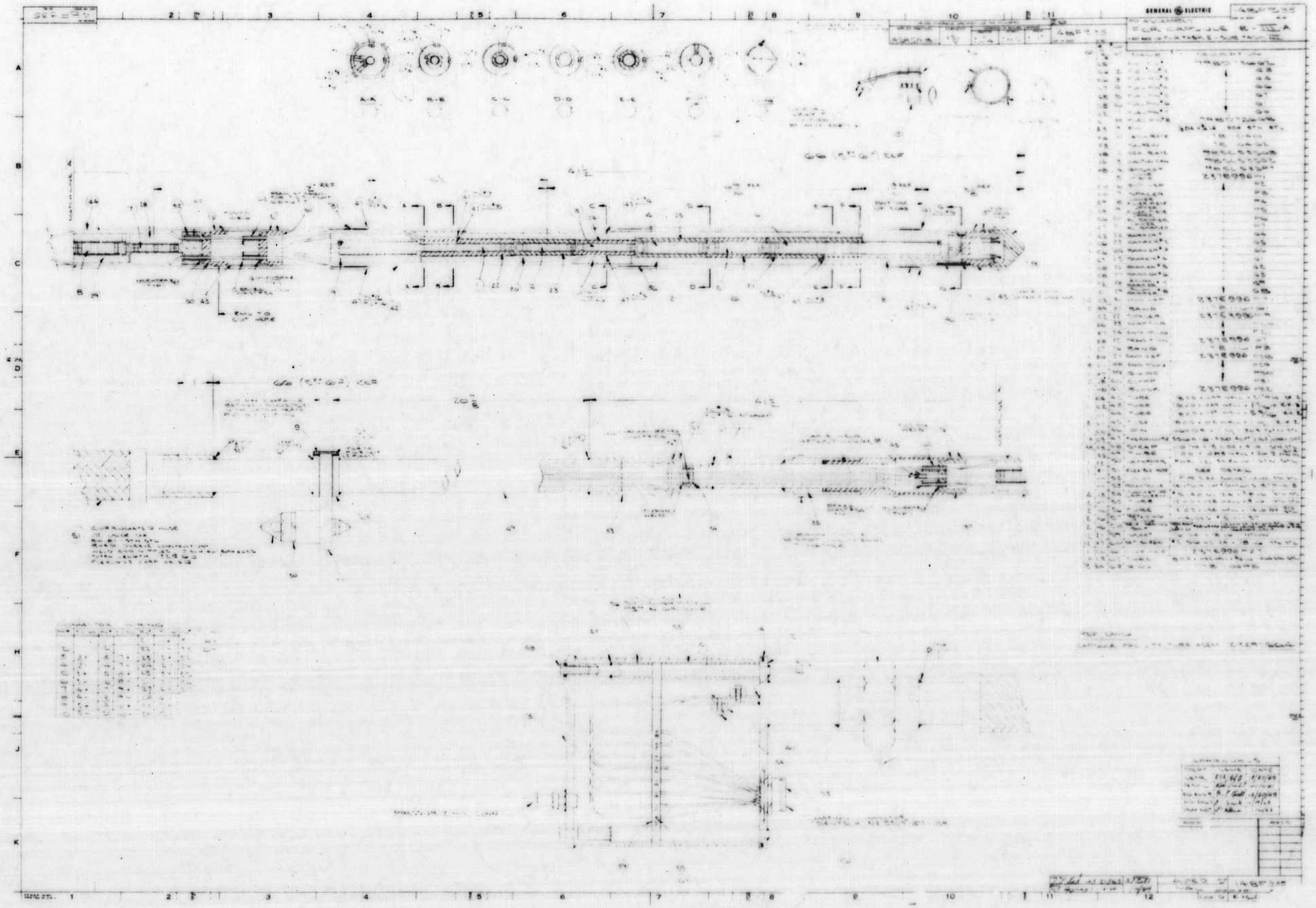

Figure 5-3. FCR Capsule E3A

This capsule is scheduled for reactor insertion in late April 1964.

Central fuel thermocouples have been eliminated from specimens 1 and 6 because of similarity in design parameters between capsule E3A and E1A. Fuel temperature estimates in E3A will be based on capsule power measurements and on the fuel temperature measurements to be made in capsule E1A.

### 5.3.2 E3A Fuel Fabrication

Approximately 15 percent of the required fuel pellets are completed. The Pu-242 content of the two homogeneously spiked thermal-demixing pellets has been increased to 5 mg/pellet to increase the sensitivity of isotope ratio measurement relative to plutonium background concentrations.

### 5.3.3 Core Drilling

Ultrasonic axial core drilling has been successfully demonstrated on both sound and cracked $UO_2$ mounted in "hysol." Specimens containing cracks of varying sizes were drilled using blade-type bits. The samples and their resulting cores are shown in Figure 5-4. Approximately 0.015 inch square cores were produced in both slightly cracked and in grossly cracked material. In addition, single cores approximately 0.020, 0.030, and 0.040 inch in diameter and from 0.1 to 0.2 inch long have been drilled from solid $UO_2$ pellets to investigate deep core-drilling techniques. This technique will be used for radial core drilling of the thermal demixing pellets.

Techniques to retrieve cores from the fuel matrix material prior to the individual linear micro sampling have been explored. Hypodermic needles were used as a retrieval shroud for 0.010 and 0.020 inch diameter wires held in a wax base. Both "push-through" and "lift" concepts were investigated and appear feasible. Additional tests are continuing to establish a reliable core-retrieval technique for hot specimens.

### 5.3.4 Out-of-Pile Plutonium Migration Experiment

An effort was made to quantitatively determine U-233 and Pu-242 diffusion in the $UO_2$ pellets by evaluation of the autoradiograph of the sectioned diffusion couple. This effort was abandoned because of the insensitivity of film-darkening techniques at low concentrations of alpha emitters in thick samples.

Samples were then taken at several distances from the original pellet interface by scratching the pellet with a sharp carbide tipped scribe and collecting the chips on "Scotch" tape. Mass spectrometric and alpha spectrum analysis of these samples indicate that both Pu and U are diffusing at comparable rates for a distance of at least 200 microns from the original interface. Precise data on alpha emitter concentration in the $UO_2$ is not available because of the crudeness of the

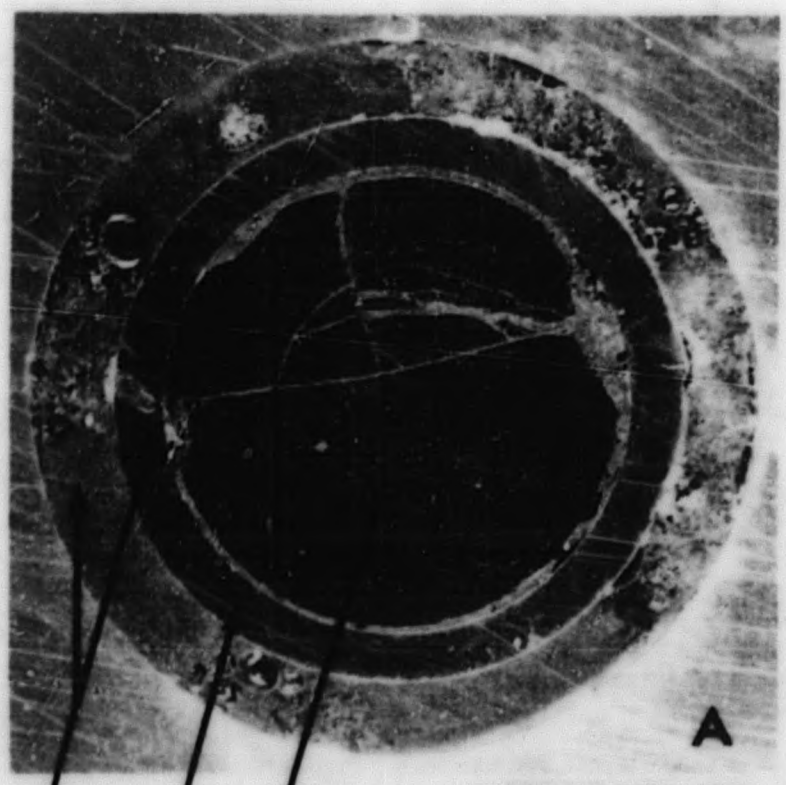


BEFORE DRILLING

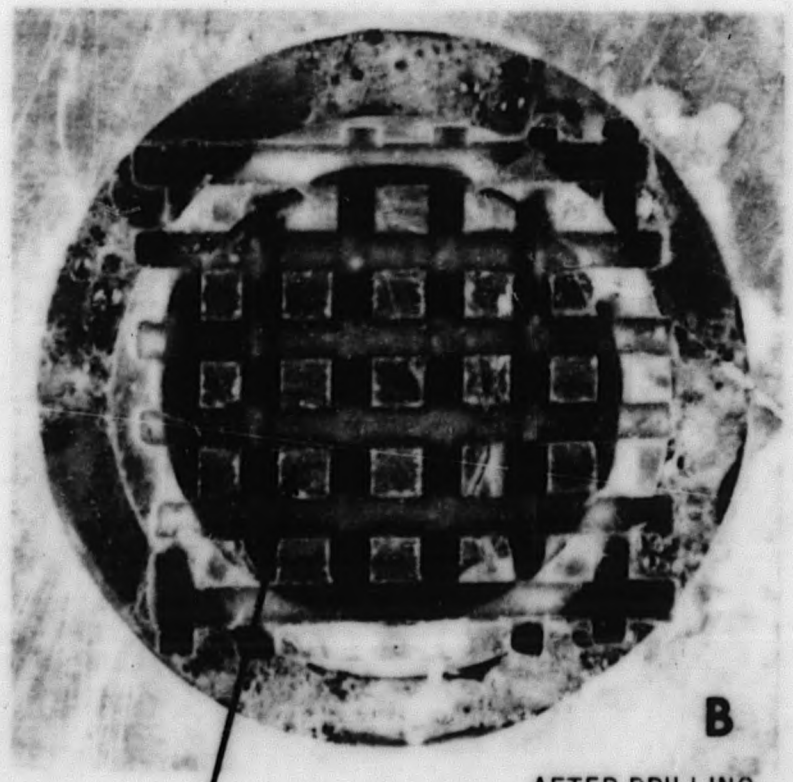


AFTER DRILLING

SLIGHTLY CRACKED SPECIMEN (0.150" O.D.)

$UO_2$

SS CLAD

"HYSOL" MOUNTING COMPOUND

0.015" x 0.015" x 0.08" $UO_2$ CORE (TYPICAL)


BEFORE DRILLING

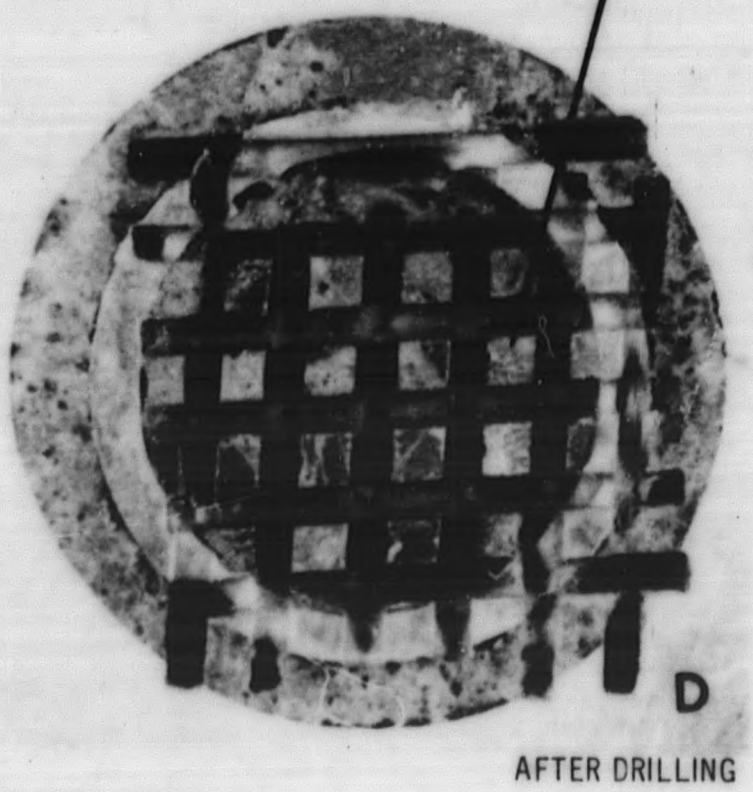


AFTER DRILLING

GROSSLY CRACKED SPECIMEN (0.150" O.D.)



Figure 5-4. Ultrasonic Drilling of Cracked $UO_2$

scratch sampling technique used. However, the results indicate a diffusion coefficient roughly consistent with published U-233 diffusion data in $UO_2$ extrapolated to the much higher temperature of this measurement.

Precision grinding equipment is being fabricated to accurately sample the out-of-pile diffusion couple and also to pilot the grinding parameters in the high-radiation-level sampling of E3A.

### 5.3.5 Mixed Oxide Compatability with Tungsten-Rhenium

High temperature tests were performed to determine the compatibility of mixed oxide fuel with tungsten-26 percent rhenium thermocouples. Specimens were made by filling 1/16 inch diameter W-26 Re tubing with crushed mixed oxide fuel pellets. One specimen contained fuel with an oxygen-to-metal ratio of 2.00 and the other an oxygen-to-metal ratio of 1.97. Both specimens were heated to 2200-2300 C for about 13 hours. They were sectioned and metallographically examined to determine if gross fuel-thermocouple reactions would occur that could effect the reliability of central fuel thermocouples. Figure 5-5 shows cross sections of the fuel and tubing for the two specimens. There is no gross alloying or attack in either specimen.

Some localized grain boundary attack was noted in a portion of the tubing containing the fuel with an oxygen-to-metal ratio of 2.00. A control sample will be examined to try to determine the origin of this attack.

## 5.4 Fuel Compositions and Properties

### 5.4.1 Autoradiography of Fuel Pellets and Pu Segregation

Mixed oxide fuei pellets with compositions ranging from one to 90 percent $PuO_2$ were prepared for examination by high-resolution autoradiography. The objective was to determine whether or not homogeneity existed throughout all compositions of pellets prepared via the coprecipitation route. It was observed from this study that mixed oxide pellets with plutonia enrichments of 11 percent and greater exhibited excellent homogeneity. Some segregation, in the form of plutonium-rich spots appeared, however, in compositions of 5.5 percent plutonia and lower.

The pellet of 5.5 percent enrichment exhibited a very few hot spots of low intensity; the apparent amount of plutonium segregated was negligible, below 0.1 percent.

The pellet of 2.22 percent enrichment showed 30 to 40 hot spots per surface in the range of 2 to 6 mils diameter and 5 percent Pu concentration. This was confirmed by examining a second surface at a ten-mil depth below the first. One 7 mil diameter spot with a 9 percent $PuO_2$ concentration was observed. The total amount of Pu segregated, however, was approximately only 1 percent of the total present.

O/M = 2.00

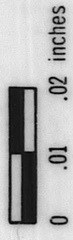


2200 – 2300°C
13 HOURS

O/M = 1.97

1660–6

Figure 5-5. Mixed Oxide in Tungsten-26 Rhenium Tubing

The pellet of 1.37 percent plutonia content showed approximately 60 hot spots on the polished planar surface in the range of two to four mils diameter and 3 percent concentration. The amount of Pu segregated was approximately 2 percent of the total Pu present.

Observations on the autoradiography study are summarized in Table V-?. Figure 5-6 shows enlarged photographs of typical low-enriched pellets which showed segregation and a 20 percent plutonia specimen which did not.

### 5.4.2 Micro Thermogravimetric Analysis

Assembly of the micro-thermogravimetric equipment has proceeded using the Cahn RG Electrobalance, a General Electric millivolt recorder, and a specially constructed furnace. The apparatus will be set up in a "cold" area and used for development of techniques prior to installation in an alpha enclosure. Requirements for design of the glove box and shielding have been delineated.

### 5.4.3 Oxygen-to-Metal Analyses

A total of 124 sintered, mixed oxide pellets (two samples from each sintering run) were analyzed for O/M ratio by the macro gravimetric method. Samples from sintering runs made with water addition to the furnace gas were consistently 1.998 to 2.000.

### 5.4.4 X-ray Analysis

Pellets of $UO_2$-20 percent $PuO_2$ mixed oxide with known oxygen metal ratios (varying from 1.97 to 2.35) have been prepared and submitted for x-ray studies. In addition, pellets of various compositions in the $UO_2$-$PuO_2$ system have been adjusted to stoichiometric O/M ratio, and will be examined by x-ray diffraction to carefully establish the relation between unit cell size and mol percent plutonia.

A number of $UO_2$-$PuO_2$ mixed oxides of various compositions have been analyzed by x-ray diffraction. These analyses have determined the extent of solid solution, the phase compositions and in addition, substantially refined the relationship between the lattice size of the solid solution and oxide composition. The lattice parameters of the various samples and other pertinent data are listed in Table V-3. These parameters were obtained from samples with an oxygen-to-metal ratio of 2.000. The compositions have been verified to be within 2 percent of the total metal atom content. Only those back-reflection diffraction peaks greater than 120 degrees $2\theta$ were used in the lattice size determinations so that a high degree of accuracy could be obtained. The plot of $a_o$ versus $UO_2$-$PuO_2$ composition is shown in Figure 5-7. It can be seen that a slight positive deviation from Vegard's straight-line relationship seems to exist. The $a_o$ values for the two end points (100 percent $UO_2$ and 100 percent $PuO_2$) however, might be questioned.

TABLE V-2
AUTORADIOGRAPHIC EXAMINATION OF
UNIRRADIATED MIXED OXIDE PELLETS

| Pellet Number | Percent $\frac{Pu}{U + Pu}$ | Observations |
|---|---|---|
| B-42-6 | 1.37 | Approximately 60 hot spots per planar surface. Spots are 2 to 4 mils diameter, 3 percent $PuO_2$ concentration. Approximately 2 percent of total Pu is segregated. |
| B-43-3 | 2.22 | 30 to 40 hot spots per surface; 2 to 6 mils diameter; 5 percent concentration. |
| B-10-3 | 5.51 | Few hot spots observed. Less than 0.1 percent of the Pu segregated. |
| B-11-3 | 11.1 | No segregation observed. |
| B-12-3 | 16.7 | No segregation observed. |
| B-8-91 | 19.9 | No segregation observed. |
| B-4-129 | 28.1 | No segregation observed. |
| B-13-3 | 39.9 | No segregation observed. |
| B-14-3 | 52.8 | No segregation observed. |
| B-15-3 | 62.0 | No segregation observed. |
| B-16-3 | 72.2 | No segregation observed. |
| B-17-3 | 81.0 | No segregation observed. |
| B-18-3 | 90.0 | No segregation observed. |

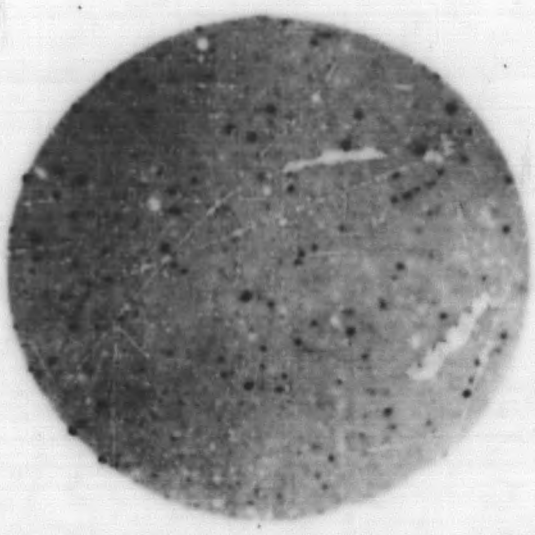

(a) $UO_2$ - 2.22% $PuO_2$
SURFACE 1 10X

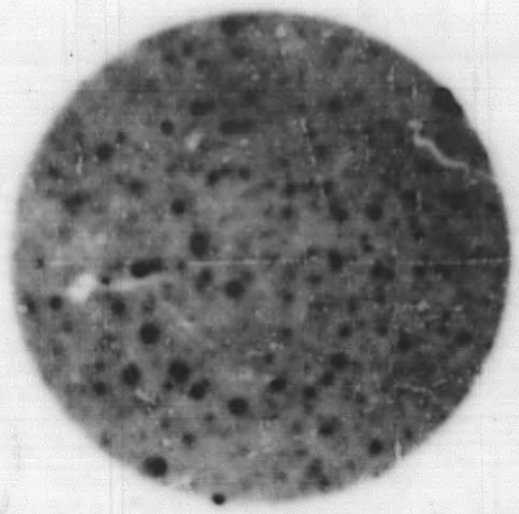

(b) $UO_2$ - 2.22% $PuO_2$
SURFACE 2 10X

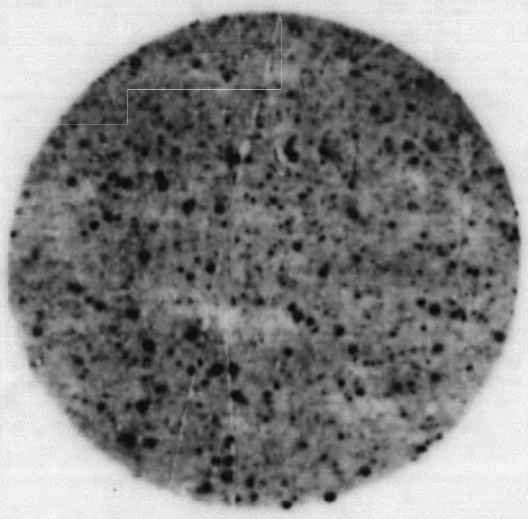

(c) $UO_2$ - 1.37% $PuO_2$
10X

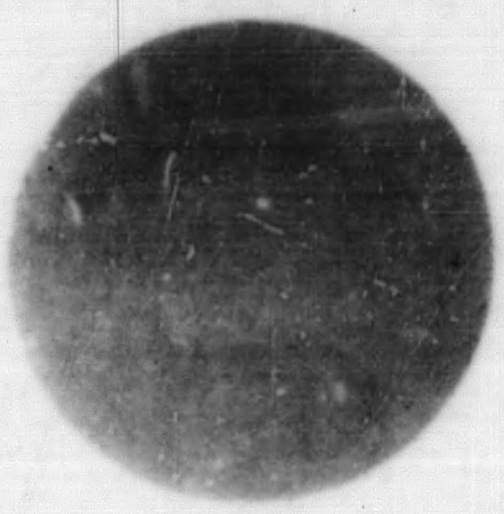

(d) $UO_2$ - 20.0% $PuO_2$
10X

**Figure 5-6. Autoradiographs of Un-Irradiated Mixed Oxide Fuel Pellets**

TABLE V-3

X-RAY DATA FOR STOICHIOMETRIC $UO_2$-$PuO_2$

| Sample Number | Pu/U+Pu | Impurities | Solid Sol. | Diff. Pattern Qual. | $a_o$ (Å) |
|---|---|---|---|---|---|
| $UO_2$ | 0 | - | - | Good | 5.4704 ± 0.0005 |
| B-10-2 | 5.51 | $Pu_2O_3$(trace) | Yes | Good | 5.466 ± 0.001 |
| B-11-2 | 11.1 | ? | Yes | Good | 5.461 ± 0.001 |
| B-12-2 | 16.7 | - | Yes | Good | 5.459 ± 0.001 |
| B-7-84 | 19.7 | - | Yes | Good | 5.4568 ± 0.0005 |
| B-5-51 | 19.9 | - | Yes | Good | 5.4571 ± 0.0005 |
| B-2-94 | 20.0 | - | ? | Poor | 5.457 ± 0.001 |
| B-3-4 | 20.6 | Unidentified (trace) | Yes | Med-Good | 5.4574 ± 0.0005 |
| B-6-45 | 22.5 | $Pu_2O_3$ | Yes | Good | 5.4547 ± 0.0005 |
| B-4-116 | 28.1 | - | Yes | Good | 5.4525 ± 0.0008 |
| B-13-2 | 39.9 | - | Yes | Good | 5.442 ± 0.001 |
| B-14-2 | 52.8 | - | Yes | Good | 5.4341 ± 0.0005 |
| B-15-2 | 62.0 | - | Yes | Good | 5.4272 ± 0.0005 |
| B-16-2 | 72.2 | - | Yes | Good | 5.4168 ± 0.0005 |
| B-17-2 | 81.0 | - | Yes | Good | 5.411 ± 0.001 |
| B-18-2 | 90.0 | ? | Yes | Good | 5.406 ± 0.001 |
| P-2-3 | 100.0 | - | - | Poor | 5.397 ± 0.0015 |

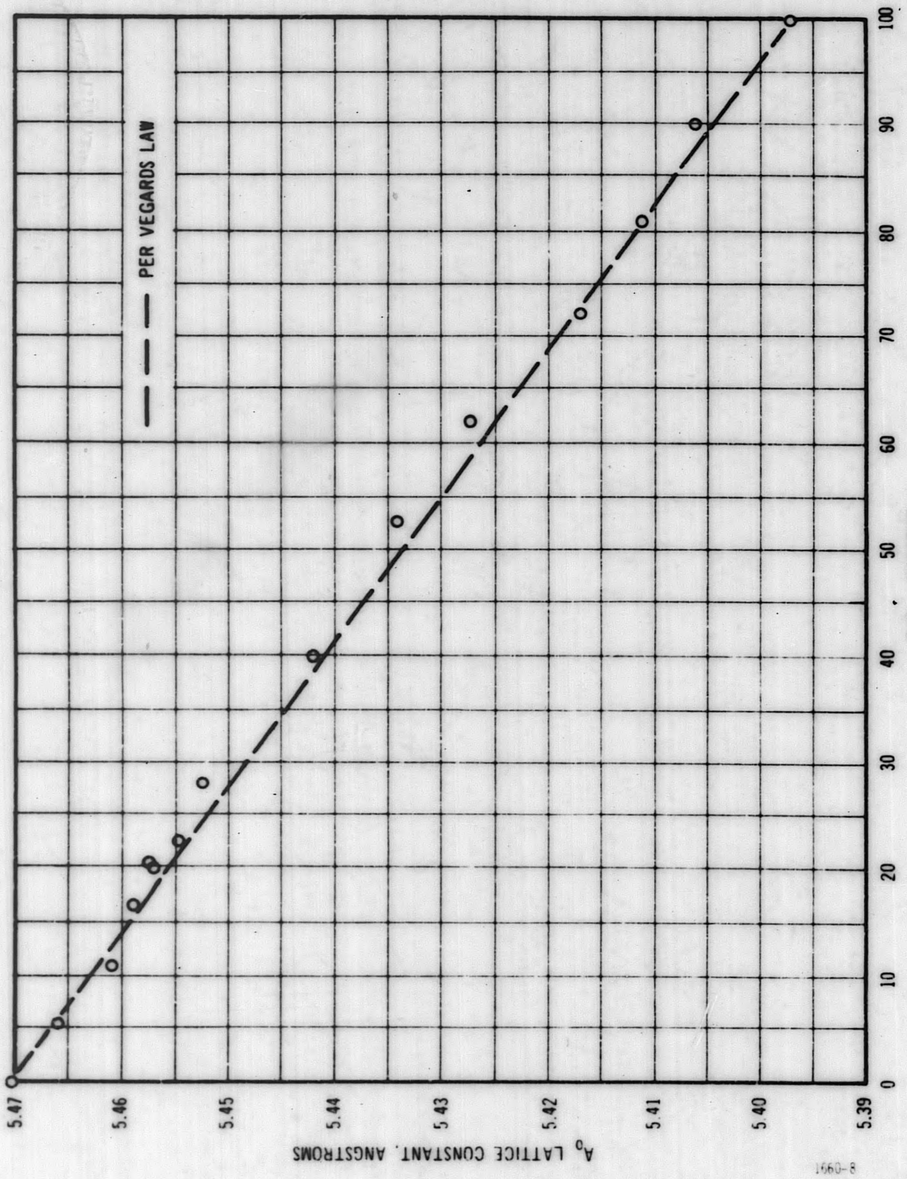


Figure 5-7 Experimental Lattice Parameters for $UO_2$-$PuO_2$ Solid Solutions

The lattice parameter for face-centered cubic $UO_2$ is listed as 5.4682Å in the ASTM x-ray data file. However, this value was not obtained from a stoichiometric specimen, but from one with an oxygen-to-uranium ratio of 2.03. When this parameter is adjusted by use of the well established equation relating lattice size to $UO_{2+x}$ ($a_x = a_o - 0.074x$), the $a_o$ for stoichiometric uranium dioxide becomes 5.4704Å, a value that has been confirmed experimentally.

The lattice parameter for $PuO_2$ was obtained from a poorly crystallized specimen and the peak positions could not be determined with the desired accuracy. This point will be re-examined using data obtained from a better specimen.

5.4.5 Fissia Synthesis

Pellets simulating fuel irradiated for 3.0 years to a peak burnup of 100,000 MWD/T have been fabricated by a cold pressing and sintering process. The sample composition is shown in Table V-4. All of the fissia additions, except cesium, were weighed in air and added to the batch in the form listed in the table. The cesium was weighed in an argon atmosphere, allowed to oxidize and hydrolize in air, and then added. The batch was mixed with a mortar and pestle and then tumbled in a twin-shell blender to gain homogeneity before pressing. Unidirectional pressing of about 10,000 psi resulted in pellets with densities of about 5.75 g/cm$^3$. These pellets, together with 2 samples of the 80 $UO_2$:20 $PrO_2$ composition (O/M = 2.00) were sintered for 6 hours in hydrogen at 1700 C. Pressing and sintering data are shown in Table V-5.

In the hydrogen sintering the fissia samples achieved about the same degree of densification as the $UO_2$-$PrO_2$ samples. During sintering the fissia pellets retained their original shapes and showed no tendency to laminate, bloat or crack. Relative weight losses during sintering indicate that some of the fission product additions were reduced during the treatment. In an attempt to increase the density of the fissia pellets a static argon atmosphere sintering treatment will be effected.

Work is continuing on the fabrication of the $UO_{2.05}$ samples for the thermal conductivity measurements. It has been found that $UO_{2.06}$ pellets of 93-95 percent theoretical density can be prepared by a combination of steam sintering and hydrogen reduction.

X-ray diffraction analysis of sample F-16 (see Table V-6) has indicated a single face-centered cubic phase with a fluorite structure with a lattice parameter of 5.4671 ±0.0002Å. This corresponds to a theoretical density of 10.29 gms/cc. The present experimental data indicates that the $UO_2$-$PrO_2$ solid solution is an excellent substitute for $UO_2$-$PuO_2$. On this basis work is being initiated to add synthetic fission to the $UO_2$-$PrO_2$ solid solution to duplicate the chemical properties of 118,000 MWD/T irradiated mixed oxide.

TABLE V-4
COMPOSITION OF FISSIA BATCH F-A (O/M = 1.88)

| Element | Elemental Weight Percent | Compound Added to Batch |
|---|---|---|
| U | 77.258 | $UO_{2.041}$ |
| Pr (for Pu) | 10.411 | $PrO_{1.833}$ |
| Rb | 0.055 | RbI |
| Sr | 0.221 | $SrO_2$ |
| Y | 0.121 | $Y_2O_3$ |
| Zr | 1.170 | $ZrO_2$ |
| Nb | 0.033 | $Nb_2O_5$ |
| Mo | 1.236 | $MoO_3$ |
| Ru | 1.579 | Ru |
| Pd | 1.060 | Pd |
| Ag | 0.121 | Ag |
| Cd | 0.077 | CdO |
| In | 0.011 | In |
| Sn | 0.022 | $SnO_2$ |
| Sb | 0.022 | $Sb_2O_3$ |
| Te | 0.386 | $TeO_2$ |
| I | 0.210 | RbI + $I_2O_5$ |
| Cs | 1.501 | Cs |
| Ba | 0.530 | $BaO_2$ |
| La | 0.462 | $La_2O_3$ |
| Ce | 1.071 | $CeO_2$ |
| Pr | 0.397 | $PrO_{1.833}$ |
| Nd | 1.479 | $Nd_2O_3$ |
| Sm | 0.464 | $Sm_2O_3$ |
| Eu | 0.055 | $Eu_2O_3$ |
| Gd | 0.011 | $Gd_2O_3$ |

TABLE V-5

SINTERING DATA FOR SYNTHETIC FISSIA

| Sample Number | Sintering Conditions: Temperature °C | Sintering Conditions: Time Hours | Pressed Dimensions: Weight gm | Pressed Dimensions: Height inch | Pressed Dimensions: Diameter inch | Pressed Dimensions: Density g/cm$^3$ | Sintered Dimensions: Weight g | Sintered Dimensions: Height inch | Sintered Dimensions: Diameter inch | Sintered Dimensions: Density g/cm$^3$ |
|---|---|---|---|---|---|---|---|---|---|---|
| F-A-1 | 1700 | 6 | 2.0654 | 0.181 | 0.393 | 5.73 | 1.9721 | 0.162 | 0.348 | 7.79 |
| F-A-2 | 1700 | 6 | 2.0707 | 0.182 | 0.393 | 5.71 | 1.9699 | 0.160 | 0.342 | 8.16 |
| F-19 | 1700 | 6 | 2.9703 | 0.254 | 0.397 | 5.75 | 2.9533 | 0.229 | 0.355 | 7.93 |
| F-20 | 1700 | 6 | 2.1166 | 0.282 | 0.396 | 5.75 | 2.1065 | 0.165 | 0.357 | 7.77 |

TABLE V-6

SINTERING DATA FOR 80 W/O $UO_2$ - 20 W/O $PrO_2$*

| Sample Number | Sintering Conditions: Temperature °C | Sintering Conditions: Time Hours | Pressed Dimensions: Weight gm | Pressed Dimensions: Height inch | Pressed Dimensions: Diameter inch | Pressed Dimensions: Density g/cm$^3$ | Sintered Dimensions: Weight g | Sintered Dimensions: Height inch | Sintered Dimensions: Diameter inch | Sintered Dimensions: Density g/cm$^3$ |
|---|---|---|---|---|---|---|---|---|---|---|
| F-16 | 1900 | 2 | 2.7533 | 0.242 | 0.392 | 5.79 | 2.5443 | 0.204 | 0.331 | 8.83 |
| F-17 | 1900 | 6 | 2.2617 | 0.197 | 0.392 | 5.79 | 2.1325 | 0.164 | 0.327 | 9.43 |
| F-18 | 1900 | 6 | 1.2036 | 0.105 | 0.392 | 5.78 | 1.1165 | 0.087 | 0.326 | 9.36 |

* Sintered in Argon

# SECTION VI

## TASK F - FAST FLUX IRRADIATION OF FUEL

### 6.1 Irradiation in EBR-II

An assembly of 19 encapsulated specimens, Group 2, is to be irradiated at high power and high burnup in EBR-II. Group 1, consisting of four specimens, is to be irradiated at high power for one cycle to obtain scoping and stability information in order to confirm placement of Group 2 in a high-power position. To shorten irradiation time, it is planned to load Group 2 to accumulate burnup at moderate power while Group 1 is being irradiated and examined.

To approach the high-power condition in a fuel element of FCR dimensions, it has been necessary to fully enrich the $UO_2$ in the mixed $PuO_2$ - $UO_2$ fuel. The specimen power to be attained is dependent on the irradiation position and the EBR-II power level, as shown in Table VI-1. The 45 MW power level is included since EBR-II is expected to operate at 45 MW for a substantial period of time before it goes to higher power.

#### Design

The specimens are to be encapsulated and then loaded into an assembly of standard design for EBR-II irradiation. The capsule has been designed, reviewed by ANL, and revised accordingly as shown in Dwg Number 798D143, Figure 6-1. The specimens to be loaded into the capsules are shown in Dwg Number 798D146, Figure 6-2.

#### 6.1.1 Statistical Design of Specimens

Within the specimen dimensions shown in Figure 6-2, there are parameters associated with fuel pellet material, the fuel clad material, and the gaps between the fuel and clad. The statistical design for specimens in Groups 1 and 2 is shown in Table VI-2. The design has been made such that the effect contributed by each of the parameters can be determined in the post-irradiation examination of Group 2 (19 specimens). Group 1, containing four specimens, is designed to provide information on selected parameters in combinations after one cycle irradiation.

#### 6.1.2 Fuel Specimen Fabrication

The special fuel clad tubing has been sized to close inside dimensions. Hardware suitable for use in loading 29 fuel specimens has been fabricated. Hardware for the 30-mil wall tube is being fabricated.

TABLE VI-1

MAXIMUM FCR SPECIMEN POWER FOR THE VARIOUS IRRADIATION POSITIONS IN EBR-II

(Based on Data from ANL, November 20, 1963)

| EBR-II Positions | Number of Subassemblies of this Description | Specimen Power in Kw/ft when EBR-II operates at 45 MW | 62.5 MW |
|---|---|---|---|
| Row - Number | | | |
| Core: ** | | | |
| 1 - 1 | 1 | 18.8* | 26.1* |
| 2 - 1 | 6 | 18.4 | 25.6 |
| 3 - 1 | 4 + 2 control rods | 17.2 | 23.8 |
| 3 - 2 | 6 | 17.5 | 24.3 |
| 4 - 1 | 6 | 15.0 | 20.8 |
| 4 - 2 and 3 | 12 | 15.9 | 22.1 |
| 5 - 1 | 6 control rods | --- | --- |
| 5 - 2 and 4 | 12 | 13.7 | 19.0 |
| 5 - 3 | 6 control rods | --- | --- |
| Inner Blanket: ** | | | |
| 6 - 1 | 6 | 11.1 | 15.4 |
| 6 - 2 and 5 | 12 | 11.2 | 15.5 |
| 6 - 3 and 4 | 12 | 12.0 | 16.7 |

* Values tabulated are those calculated for pin nearest the center. Depending on the position, other pins can have as much as 15 percent less power.

** The test subassembly is interchangeable in the positions of the core and in the positions in the inner blanket, but not between the core and the inner blanket positions.

TABLE VI-2

STATISTICAL DESIGN FOR EBR-II IRRADIATION

| Pin | Fuel O/M | Axial Gap | Blanket Percent $U^{235}$ | Fuel Bulk Density | Clad Wall Thickness | Clad Material | Radial Gap | Fuel Enrichment | Purpose of Pin |
|---|---|---|---|---|---|---|---|---|---|
| Group 1 | | | | | | | | | Short Term, High Power |
| 1-A | 2.000 | Standard | Natural | --- | 0.015 inch | 347 | Standard | Full | (Parameters in |
| 1-B | 2.000 | Standard | Natural | Normal/Above Normal/Above | 0.015 inch | 347 | Standard 0.001 inch | Full | sections as shown) |
| 1-C | 2.03 | 0.002 inch | Natural | Normal/Above Normal/Above | 0.015 inch | Incoloy | Standard | Full | |
| 1-D | 1.97 | Standard | Natural | Normal/Above Normal/Above | 0.015 inch | 316 | Standard 0.001 inch | Full | |
| Group 2 | | | | | | | | | High Burnup - 100,00 MWD/T |
| 2-A | 2.000 | Standard | Natural | Normal | 0.015 inch | 347 | Standard | Full | |
| 2-B | 2.000 | Standard | 25% | Normal | 0.015 inch | 316 | Standard | Full | |
| 2-C | 2.000 | 0.002 inch | Natural | Normal | 0.015 inch | Incoloy | Standard | Full | |
| 2-D | 2.000 | 0.002 inch | 25% | Normal | 0.015 inch | 347 | Standard | Full | |
| 2-E | 1.97 | Standard | Natural | Normal | 0.015 inch | 316 | Standard | Full | |
| 2-F | 1.97 | Standard | 25% | Normal | 0.015 inch | Incoloy | Standard | Full | Statistical Design |
| 2-G | 1.97 | 0.002 inch | Natural | Normal | 0.015 inch | 347 | Standard | Full | for Parameters |
| 2-H | 1.97 | 0.002 inch | 25% | Normal | 0.015 inch | 316 | Standard | Full | |
| 2-J | 2.000 | Standard | Natural | Above Normal | 0.015 inch | Incoloy | Standard | Full | |
| 2-K | 2.000 | 0.002 inch | 25% | Above Normal | 0.015 inch | 347 | Standard | Full | |
| 2-L | 1.97 | Standard | 25% | Above Normal | 0.015 inch | 316 | Standard | Full | |
| 2-M | 1.97 | 0.002 inch | Natural | Above Normal | 0.015 inch | Incoloy | Standard | Full | |
| 2-N | 2.000 | Standard | Natural | Normal/Above | 0.010 inch | 347 | Standard | Full | Thin clad wall |
| 2-O | 2.03 | Standard | Natural | Normal/Above | 0.015 inch | 347 | Standard | Full | High O/M |
| 2-P | 2.000 | Standard | Natural | Normal/Above | 0.015 inch | 347 | Standard | 40 percent $\frac{U^{235}}{U}$ | Reduced power |
| 2-Q | 2.000 | Standard | Natural | Normal/Above | 0.015 inch | 347 | 0.001 inch | Full | Close pellet-clad gap |
| 2-R | 2.000 | 0.002 inch | Natural | Normal/Above | 0.015 inch | 347 | 0.001 inch | Full | Combined close gap |
| 2-S | 2.000 | 0.002 inch | Natural | Normal/Above | 0.030 inch | 347 | 0.001 inch | Full | Thick wall clad |
| 2-T | | To be Determined | | | 0.015 inch | 316 | Standard | Full | Fuel parameters to be determined |

Blanket pellets are complete except for the 25 percent enriched pellets.

Specimens have been assembled in accordance with statistical design in Table VI-2, and current status is as follows:

1. Pin 1-A completed as reported previously.

2. Pins 1-B, 2-A, and 2-N were welded, leak checked, and transferred to RML for pre-irradiation examination.

3. Pins 2-C, 2-J, and 2-P were loaded and welded.

4. Pins 2-Q and 2-R are ready for loading.

In addition to the pellets in the above pins, sintered pellets are available for approximately 10 more pins.

### 6.1.3 Sodium Fill System Fabrication

The mechanical and electrical work on the sodium fill system is essentially complete. Fabrication of the dummy capsules has been completed. The sodium for testing the sodium fill system has been received. Following loading of the dummy capsules, one will be sent to the RML for a practice destructive examination.

Next month, fabrication of the sodium fill system will be completed and checkout begun. The revised operating instructions will be issued. Eddy current testing equipment will be set up.

### 6.1.4 Capsule Fabrication

Capsule material which will be exposed to EBR-II coolant is to be supplied by ANL. This material, scheduled for delivery to General Electric - December 16, was found to contain flaws when received from the vendor by ANL and had to be re-ordered. Meanwhile, as possible backup, tubing purchased by General Electric for an earlier irradiation design is being shipped to ANL for their examination for possible use for the capsules.

Since no fabrication on the capsules for the specimens can be initiated without the tubing material, this item is now critical on the schedule for their completion.

### 6.1.5 Planning for Group III

Consideration has been given to the design of the Group III fuel preparatory to discussing the design with ANL. The unencapsulated feature will require a departure from the "standardized" capsule design. The characteristics desired are:

1. Unencapsulated - exposure of the fuel clad to flowing sodium.

2. Intermediate fuel burnup.

3. Exposure of the fuel clad at temperatures from 700 to 1300 F. Two methods for attaining the higher temperature are:

   a. Using an orifice to reduce flow.

   b. Using a thermal dam to raise the clad temperature.

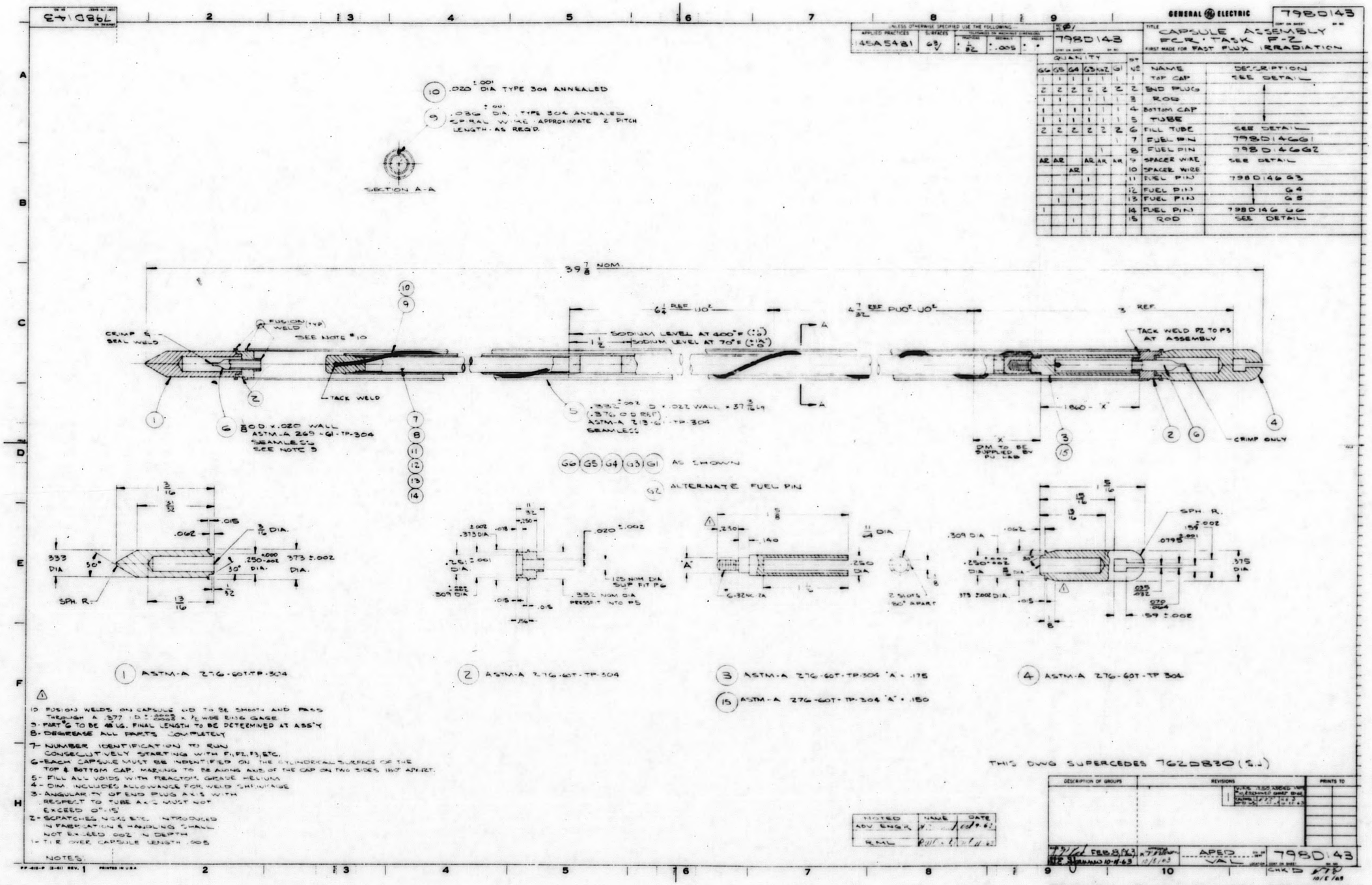


Figure 6-1. Capsule Assembly - FCR Task F-2

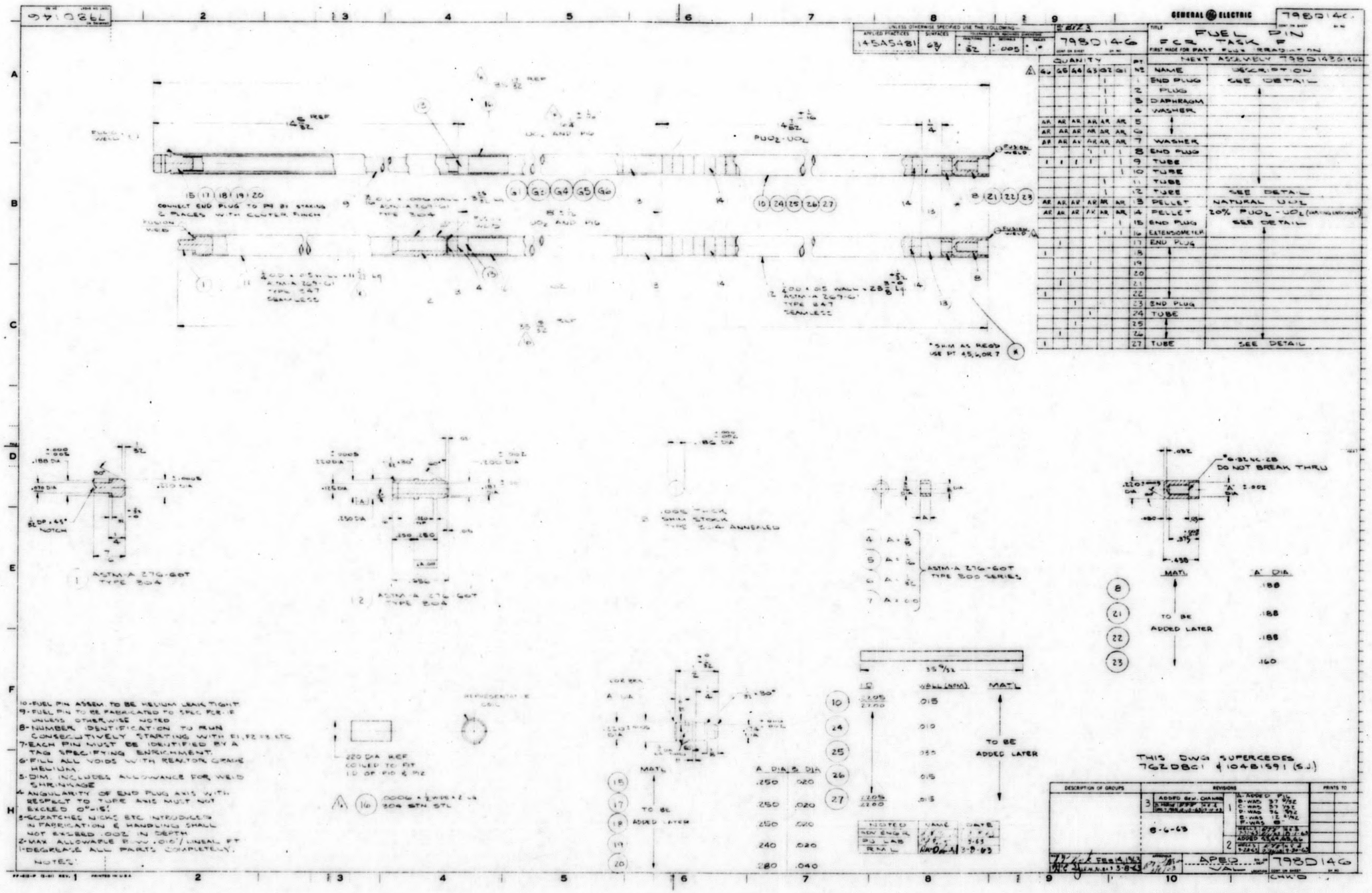


Figure 6-2. Fuel Pin - FCR Task F

# SECTION VII

## TASK G - REACTOR PHYSICS AND CORE ANALYSIS

### 7.1 U-238 - Pu-239 Resonance Overlap Effect

The computer code DOPIE,[2] which computes group average cross sections by taking

$$\bar{\sigma}_j = \frac{\int_{E_1}^{E_2} \frac{S(E)\,\sigma_i(E)}{\sigma_t(E)}\,dE}{\int_{E_1}^{E_2} \frac{S(E)\,dE}{\sigma_t(E)}}. \qquad (1)$$

where S(E) is a scattering source at energy E. $\sigma_i(E)$ includes resonance contributions of the isotope i only, and $\sigma_t(E)$ includes resonance contributions of all the fuel isotopes, was used to obtain temperature-dependent cross sections of U-238 and Pu-239 in the important Doppler energy range of a large fast ceramic reactor (200 to 2000 Kev). With the Pu-239 resonances being unresolved in this energy range, an averaging technique was used to obtain plutonium cross sections and their Doppler changes. Since all resonances in the DOPIE calculation are treated as if they are resolved, a sampling of 15 equally probable Pu-239 resonances, representing the appropriate distributions[9] for and producing the correct average of the resonance parameters was used. The order and placement of these 15 resonances was randomly selected for each 37.5 ev interval, with an average spacing of 2.5 ev. Several runs were made over the energy range from 800 to 1000 ev, differing only in the placement and order of the Pu-239 resonances. By randomly selecting the order and placement for each run, some insight was gained into the range of uncertainty the Pu-239 Doppler effect has due to lack of resolved resonances. Table VII-1 shows the extreme variation possible in the Pu-239 Doppler effect resulting from reordering the resonances while maintaining the correct distributions and average parameters. As might be expected, the fission and capture Doppler effects do not vary in the same way.

TABLE VII-1

Pu-239 CROSS SECTIONS WITH U-238 RESONANCE OVERLAP EFFECTS FOR 5 RANDOM RESONANCE ORDERS

| Distribution | $\sigma_f$ 1400 K | $\sigma_c$ 1400 K | $\Delta\sigma_f$ 1400→700 K | $\Delta\sigma_c$ 1400→700 K |
|---|---|---|---|---|
| 1 | 7.541 | 4.212 | 0.065 | 0.020 |
| 2 | 7.774 | 4.333 | 0.210 | 0.118 |
| 3 | 7.605 | 4.423 | 0.467 | 0.213 |
| 4 | 7.556 | 4.402 | 0.329 | 0.181 |
| 5 | 7.354 | 4.140 | 0.178 | 0.184 |

In order to obtain a Doppler effect for Pu-239 in this energy range which is averaged over all possible resonance orders and spacings, it would be necessary to run many distributions of the type used for Table VII-1.

A more systematic averaging of the ordering and spacing of the Pu-239 cross section than one would obtain from random choice is desirable. This can be done by taking one of the fifteen resonances at a time, assuming all the Pu-239 resonances in the energy interval are of this type (2.5 ev apart) and running five successive problems for each, each time shifting the array of Pu-239 resonances by 0.5 ev with respect to the resolved U-238 resonances. This was found to be a formidable task, requiring large amounts of computer time, so only three Pu-239 resonances were run in the expectation that the flux is basically determined by the U-238 resonances and nearly independent of the weaker Pu-239 resonance used. Figure 7-1 shows the result of these runs. In each curve all (~80) of the Pu-239 resonances were taken to have the parameters indicated and spaced 2.5 ev apart. The orientation index S was set at zero when one Pu-239 resonance peak was exactly at 1 Kev. In all cases this gave an "effective" Pu-239 Doppler change slightly less (more negative) than the normal Pu-239 Doppler for that resonance. As the array of Pu-239 resonances was shifted by increments of 0.5 ev, their orientations with respect to the U-238 resonances became such that the overlapping effect resulted first in more negative and then more positive "effective" Dopplers. Averaging these results over S from zero to 2.5 ev, however, indicates that there is very little change from the normal Doppler effect for all Pu-239 resonances.

Capture cross sections for U-238 in the energy range from 200 to 1800 ev have also been computed using DOPIE. Equation (1) represents an improved calculation over those previously performed since the source had been taken to be constant in energy and the denominator was approximated by $\Delta E/\sigma_p$.

Two sets of resolved resonance parameters have been considered; those which were used previously and are resolved up to Kev, and a new set reported by Firk[10] et al., which include

values up to 1.8 Kev. The 1400 K cross sections computed in the DOPIE manner with the old parameters are essentially the same as previously obtained from RAPTURE calculations. However, the Doppler changes in these cross sections are greater by 10 to 20 percent due to the improved flux averaging and source calculation in the DOPIE code.

These increased Doppler cross sections produce about an 18 percent more negative U-238 Doppler coefficient in a large fast reactor. Use of the resolved parameters reported by Firk et al., increases the U-238 capture cross section in some groups and decreases it in others with a slight decrease in total U-238 captures. The Doppler coefficient obtained with these data is about 10 percent less negative than that obtained with the old parameters. Thus, the Doppler coefficient as computed by DOPIE with Firk's data is only 8 percent higher than the value obtained from RAPTURE[9] with the old parameters.

From these results it may be concluded that:

1. Since the flux shape is determined predominantly by the strong U-238 resonances, flux averaging of the Pu-239 cross sections with rigorous averaging techniques for the unresolved resonances results in virtually no change in the Pu-239 Doppler cross sections from that obtained for Pu-239 alone.

2. There is quite a large range about this average, making it possible to have significant deviations from this average over small energy ranges, depending upon the actual distribution of the Pu-239 resonances. Statistical probabilities for these deviations have not been determined but it is expected that a large deviation from the normal Pu-239 Doppler coefficient is not very probable.

3. All other cross sections should be flux averaged in a like manner for all materials, the most significant change of which will be an increase (~10 to 20 percent) in the U-238 Doppler effect.

## 7.2 Physics Methods Development

Physics methods development is presently centered on the completion of the TRAN-EICA codes, along with a suitable cross section file, and the specifying of a 2-dimensional synthesis diffusion code.

Coding of the instructions for the EICA code is completed and checkout has begun. Several changes in both TRAN, the cross section generator, and EICA, a zero-dimensional hyper-fine diffusion theory code which uses TRAN output, were found to be necessary. The most significant change concerns a more detailed computation of energy transfer due to elastic scattering. This was found to be necessary at high neutron energies.

Work has begun on the development of a multigroup two-dimensional diffusion theory synthesis computer code which is expected to be less expensive to run than present multigroup two-dimensional diffusion theory codes. The calculation is based on the method described by Kaplan,[11] in which the multigroup fluxes are expanded into series whose terms contain spatially separable functions, i. e. ,

$$\phi(r, z) = \sum_i a_i R_i (r) Z_i (z)$$

Two approaches are now being considered. The first involves running several one-dimensional flux solutions in one spatial variable, integrating over that variable and obtaining a solution in the other dimension. In the second approach one-dimensional flux solutions would be run in both dimensions, integrations performed in both dimensions, and the final calculation would reduce to solving simultaneous linear equations. The second approach appears to be especially well suited to fuel cycle calculations where flux changes due to burnup could be computed by just obtaining a new solution to the simultaneous equations.

A study of fission product depletion was completed during the quarter. Physics calculations for fast reactors to date have ignored the depletion of long-lived fission products due to neutron capture. The ratio of the fission product cross section with depletion in fuel at the average burnup to the cross section without depletion at half burnup (the value used in FCR studies) was computed for neutron energies from 100 ev to 1 Mev and fuel discharge burnups of up to 200,000 MWD/t. This ratio takes the form

$$R(E) = \frac{\Sigma'_a (E)}{\Sigma_a (E)} = \frac{\frac{1}{BU^f} \int_o^{BU^f} \sum_{m=1}^{M} N'_m (BU)\, \sigma_{a,m} (E)\, dBU}{1/2 \sum_{m=1}^{M} N_m (BU^f)\, \sigma_{a,m} (E)}$$

where $BU^f$ is the design burnup, m denotes an individual isotope contributing to long-lived fission product captures, $\sigma_{a,m}(E)$ is the absorption cross section of isotope m, and $N'_m(BU)$ and $N_m(BU)$ are the nuclear densities of isotope m at burnup BU with and without depletion, respectively.

Cross sections and yields of the individual isotopes making up the long-lived fission products were taken from values reported by Greebler, Hurwitz and Storm.[12] The cross sections were upgraded to correspond to the higher aggregate values of Moldauer.[13]

Figure 7-2 shows the values of R as a function of neutron energy for the reference FCR design for fuel discharged at 25, 50, 100 and 200 thousand MWD/t. For fuel discharged at 100,000 MWD/t the error in reactivity due to ignoring fission product depletion would be around 0. 3

percent, while at 200,000 it may get as high as 1 percent. This computation ignores the effects of daughter fission product isotopes, which, if included, would make these percentages lower. The reactivity error in ignoring fission product depletion is small for fuel burnup up to 100,000 MWD/t. While it should be a design consideration at 200,000 MWD/t, it is not great enough to product a significant reduction in excess reactivity.

## 7.3 FORE Code Modifications

An analysis of sodium boiling and expulsion from coolant channels has been started. It is intended to eventually incorporate this calculation, together with the accompanying reactivity feedback into the FORE transient computer code. Other improvements and revisions will be made in the FORE code at the same time.

## 7.4 The Effect of the Doppler Coefficient on the Meltdown Accident in a Fast Reactor

The influence of the Doppler effect in the core disassembly process following a meltdown accident was examined with a Bethe-Tait type model in which the Doppler effect, as well as core disassembly, has been considered in the reactor shutdown process. The work was described in detail and published in GEAP-4420.[14]

The present work has shown that a negative Doppler effect of the magnitude calculated for these large power reactors can reduce the energy release by factors of 10 or more so that the containment problem again becomes manageable.

Other conclusions are:

1. In the presence of a strong negative Doppler effect, the energy release per unit mass of core becomes essentially independent of the reactor parameters and depends only on the inserted reactivity at the point where substantial pressure buildup is initiated.

2. In the presence of a strong Doppler effect, the energy release from the meltdown accident can be terminated by a relatively low pressure buildup. The pressure-energy relation must, therefore, be understood for temperatures well below those normally of importance in the absence of a Doppler coefficient.

3. If one relies on the Doppler effect to reduce the energy release, it is advantageous to have a short neutron lifetime. This is because the energy release depends only on the inserted reactivity at the threshold of pressure generation. The inserted reactivity, on the other hand, assuming a reactivity ramp insertion, will increase with increasing neutron lifetime, as shown by McCarthy, et al.[14]

4. In the presence of a strong Doppler effect, the energy release goes linearly with reactor mass. The energy per unit mass does not increase as (McCarthy, et al., indicate) would be the case with no Doppler coefficient.

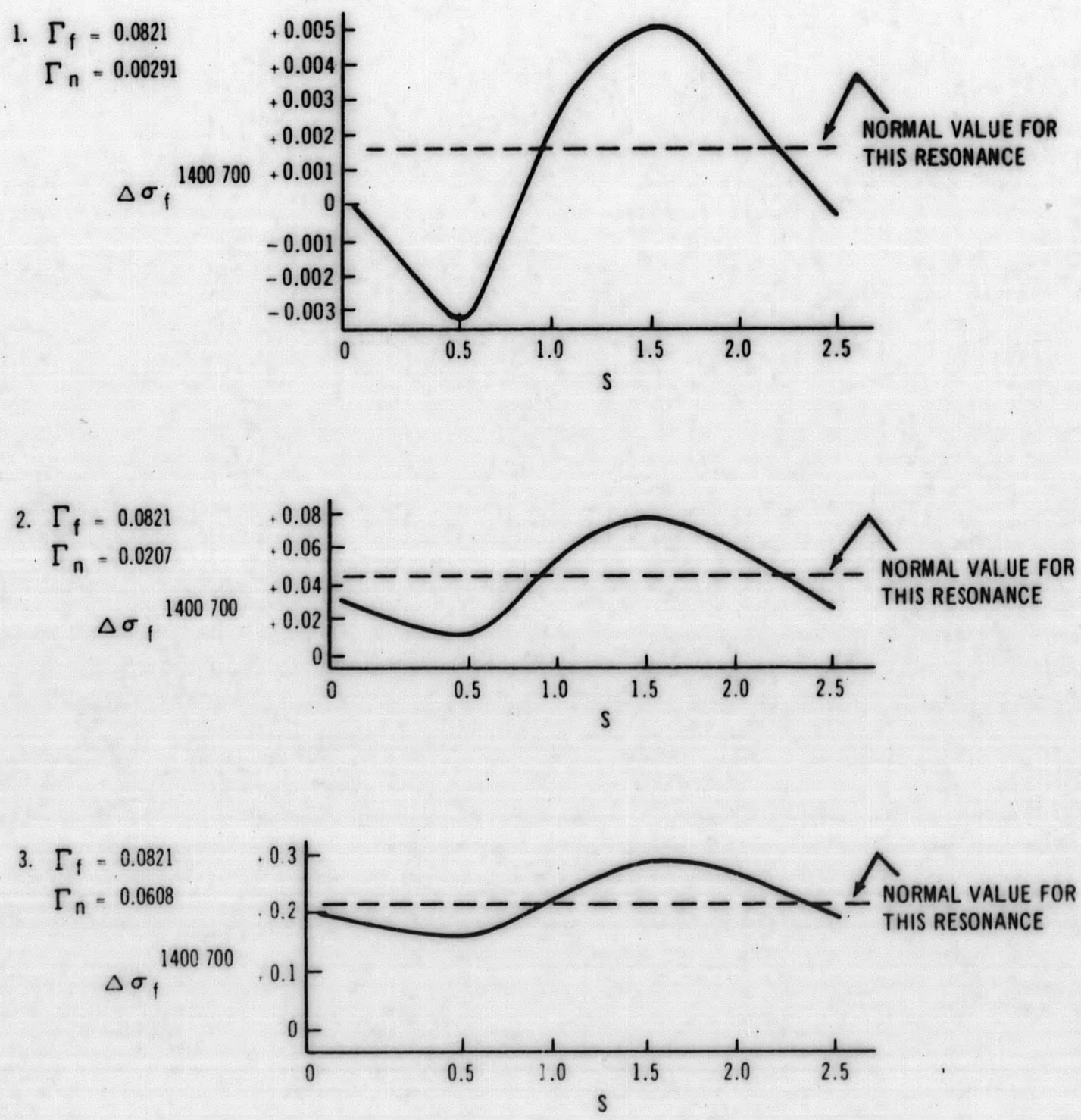


Figure 7-1. The "Effective" Doppler Change in the Fission Cross Section of Arrays of Three Plutonium$^{239}$ Resonances as a Function of Uranium$^{238}$ - Plutonium$^{239}$ Resonance Orientation

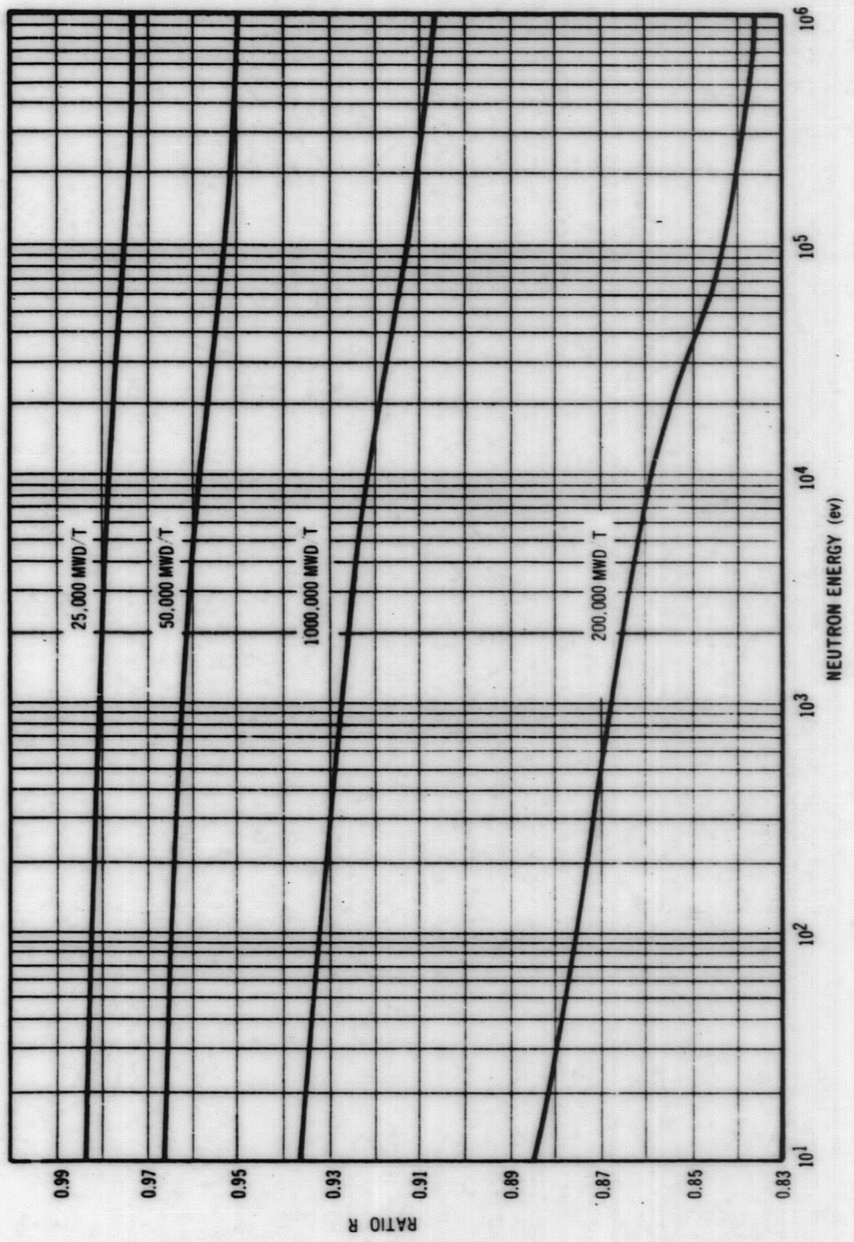


Figure 7-2. The Ratio of R as a Function of Neutron Energy for the Reference Design

## REFERENCES


1. "Fast Ceramic Reactor Development Program," Seventh Quarterly Report, April - June, 1963, GEAP-4300.

2. "Fast Ceramic Reactor Development Program," Eighth Quarterly Report, July - September, 1963, GEAP-4382.

3. Letter from H. Lawroski to J. H. Field, July 29, 1963.

4. Jakob, M., Heat Trasfer, 4th Ed., Wiley and Sons, Inc., N. Y., 1955, Chapter 13, pg. 251-284.

5. Heisler, M. P., "Temperature Charts for Induction and Constant-Temperature Heating," ASME Trans., Vol. 69, No. 3, April 1947, Figure 1 and 2, page 228, Part 2, pg. 233.

6. Salmon, M. A., "Effects of Tube Leaks in Sodium-Heated Steam Generators," NAA-SR-8140, pp. 59-86.

7. Zabel, H. R., "Containment of Fragments from Runaway Reactor," SRIA-1.

8. Lieberman, P., "Shock Impingement Experiments on Crushable Solids," ARF 4132-10, June 1959.

9. Ferziger, J. H., Greebler, P., Kelley, M. D., Walton, J., "Resonance Integral Calculations for Evaluation of Doppler Coefficients - The RAPTURE Code," GEAP-3923, June 12, 1962.

10. Firk, F. W. K., Lynn, J. E., Moxon, M. C., "Resonance Parameters of the Neutron Cross Section of U-238," Nuclear Physics, 41, pp. 614-629 (1963).

11. Kaplan, S., "Some New Methods of Flux Synthesis," Nuclear Science and Engineering, 13, 22-31 (1962).

12. Greebler, P., Hurwitz, H. Jr., Storm, M. L., "Statistical Evaluation of Fission-Product Absorption Cross Sections at Intermediate and High Energies," KAPL-P-1818, August 17, 1956.

13. Moldauer, P. A., "On the Estimation of Fast Neutron Cross Sections," ANL-6122, Proceedings on the Conference on the Physics of Breeding, October 19-21, 1959.

## REFERENCES

14. Wolfe, B., Friedman, N., Riley, D., "Influence of the Doppler Effect on the Meltdown Accident," GEAP-4420, November 18, 1963.

15. McCarthy, W. J., Nicholson, R. B., Okrent, D., Jankus, V. Z., "Studies of Nuclear Accidents in Fast Power Reactors," Paper 2165, 2nd Geneva Conference, 1958.

GEAP-4480
Informal Research
and Development Report

EDITED BY:

F. J. Leitz, Deputy Project Engineer
Fast Ceramic Reactor Program

APPROVED:

K. P. Cohen, Project Engineer
Fast Ceramic Reactor Program

END